2013

# Characterization and Aerosol Dispersion Performance of Spray-Dried Chemotherapeutic PEGylated Phospholipid Particles for Dry Powder Inhalation Delivery in Lung Cancer

Samantha A. Meenach
*University of Rhode Island*, smeenach@uri.edu

Kimberly W. Anderson

J. Zach Hilt

Ronald J. McGarry

Heidi M. Mansour



## Citation/Publisher Attribution

Meenach, S. A., Anderson, K. W., Hilt, J. Z., McGarry, R. C., & Mansour, H. M. (2013). Characterization and aerosol dispersion performance of advanced spray-dried chemotherapeutic PEGylated phospholipid particles for dry powder inhalation delivery in lung cancer, European Journal of Pharmaceutical Sciences, 49(4), 699-711. doi: 10.1016/j.ejps.2013.05.012
Available at: http://dx.doi.org/10.1016/j.ejps.2013.05.012

# Characterization and Aerosol Dispersion Performance of Spray-Dried Chemotherapeutic PEGylated Phospholipid Particles for Dry Powder Inhalation Delivery in Lung Cancer

# Characterization and Aerosol Dispersion Performance of Spray-Dried Chemotherapeutic PEGylated Phospholipid Particles for Dry Powder Inhalation Delivery in Lung Cancer

Samantha A. Meenach[1,2], Kimberly W. Anderson[2,3], J. Zach Hilt[2,3], Ronald C. McGarry[4], Heidi M. Mansour[1,3,*]

[1]University of Kentucky, College of Pharmacy, Department of Pharmaceutical Sciences - Drug Development Division, Lexington, KY 40536-0596, USA
[2]University of Kentucky, College of Engineering, Department of Chemical and Materials Engineering, Lexington, KY 40506-0046, USA
[3]University of Kentucky, Center of Membrane Sciences, Lexington, KY, USA
[4]University of Kentucky College of Medicine, Department of Radiation Medicine, Lexington, KY 40536-0284, USA

***Submission to European Journal of Pharmaceutical Sciences***

[*]***Corresponding Author:*** Heidi M. Mansour, Ph.D., R.Ph., Assistant Professor of Pharmaceutics & Drug Delivery, Faculty Associate-UK Center of Membrane Sciences, University of Kentucky, College of Pharmacy, Department of Pharmaceutical Sciences-Drug Development Division, 789 S. Limestone Street, Lexington, KY 40536-0596, USA. Phone: (859) 257-1571. Fax: (859) 257-7564. Email heidi.mansour@uky.edu

## ABSTRACT

Pulmonary inhalation chemotherapeutic drug delivery offers many advantages for lung cancer patients in comparison to conventional systemic chemotherapy. Inhalable particles are advantageous in their ability to deliver drug deep in the lung by utilizing optimally sized particles and higher local drug dose delivery. In this work, spray-dried and co-spray dried inhalable lung surfactant-mimic PEGylated lipopolymers as microparticulate/nanoparticulate dry powders containing paclitaxel were rationally designed via organic solution advanced spray drying (no water) in closed-mode from dilute concentration feed solution. Dipalmitoylphosphatidylcholine (DPPC) and dipalmitoylphosphatidylethanolamine poly(ethylene glycol) (DPPE-PEG) with varying PEG chain length were mixed with varying amounts of paclitaxel in methanol to produce co-spray dried microparticles and nanoparticles. Scanning electron microscopy showed the spherical particle morphology of the inhalable particles. Thermal analysis and X-ray powder diffraction confirmed the retention of the phospholipid bilayer structure in the solid-state following spray drying, the degree of solid-state molecular order, and solid-state phase transition behavior. The residual water content of the particles was very low as quantified analytically Karl Fisher titration. The amount of paclitaxel loaded into the particles was quantified which indicated high encapsulation efficiencies (43-99%). Dry powder aerosol dispersion performance was measure *in vitro* using the Next Generation Impactor™ (NGI™) coupled with the Handihaler® dry powder inhaler device and showed mass median aerodynamic diameters in the range of 3.4 – 7μm. These results demonstrate that this novel microparticulate/nanoparticulate chemotherapeutic PEGylated phospholipid inhalation aerosol platform has great potential in lung cancer drug delivery.

**KEYWORDS:**

Dry Powder Inhaler (DPI); Respiratory Drug Delivery; Biocompatible Biodegradable Lipopolymers; Nanotechnology; Nanomedicine; Lung Surfactant; Self-assemblies; Paclitaxel; anticancer; DPPC/DPPE-PEG; Particle Engineering

## 1.1 INTRODUCTION

Inhalation aerosol delivery dates back to ancient times (Hickey and Mansour, 2009; Patton and Byron, 2007) and aerosol formulations have been investigated for many pulmonary diseases including lung infections, cystic fibrosis, chronic obstructive pulmonary disease (COPD), and lung cancer (Arnold et al., 2007; Cartiera et al., 2010; Meenach et al., 2012a; Watts et al., 2008; Wu et al., 2010; Yang et al., 2009). The lung is an ideal target for drug delivery owing to the potential to avoid first-pass metabolism, enable a more rapid onset of therapeutic action, high local drug concentrations within the lung, and minimization of systemic absorption of the drug allowing for decreased side effects (Carvalho et al., 2011; Gill et al., 2007; Hickey and Mansour, 2008; Mansour et al., 2009; Sharma et al., 2001; Vaughn et al., 2006). Additionally, for many drugs delivery via intravenous or oral administration routes often result in high systemic drug concentrations while a relatively low amount of the drug actually reaches the lung (Carvalho et al., 2011; Vaughn et al., 2006). Specifically for lung cancer, it has been shown that drug concentrations in lung tumors are often low after systemic administration of chemotherapeutics which could be a cause of treatment failure and in some cases, the initiation of chemotherapeutic resistance (Gagnadoux et al., 2008).

In addition to the general advantages of aerosolized chemotherapy formulations, inhalable dry powder formulations offer further improvements in the treatment of lung cancer. This includes the ability to design the particle size and amount of drug loaded into the system, enhance solubility of the drug, and improve dry state storage allowing for long-term stability (Mansour et al., 2009; Sung et al., 2007). In this study, dry powder nanoparticle/microparticle formulations were designed via dilute organic solution advanced spray drying in closed-mode which has been optimized by our group for the delivery of therapeutics to treat various lung

diseases (Hayes et al., 2011; Li et al., 2011; Li and Mansour, 2011; Meenach et al., 2012b). Spray drying (SD) is an advanced high-throughput pharmaceutical manufacturing process which can design and efficiently produce respirable particles in the solid-state (Hickey and Mansour, 2008; Kikuchi et al., 1991; Mansour et al., 2009; Mansour et al., 2011). One of the advantages of using SD is that it can allow for the controlled production of particles in terms of their size, morphology, and aerosol performance characteristics. Particle engineering is particular important for pulmonary delivery where many factors impact the performance of a particle system including the aerodynamic diameter (MMAD), particle size distribution, dispersibility, morphology, and thermodynamic stability (Chow et al., 2007; Hickey et al., 2007b). In particular, previous research has shown the effect that both size and surface roughness has on particle performance where particles with MMADs 1-2 μm deposit in the smaller (lower) airways and 5-10 μm deposit in the larger (upper) airways (Vehring et al., 2007) and particles with increase surface roughness may have increased dispersibility properties due to decreased interparticulate interactions between the particles (Gilani et al., 2005).

While aerosol dry powder formulations utilizing polymers such as poly(lactic-co-glycolic) (PLGA) (Tomoda et al., 2009) and poly(ethylene glycol)-co-poly(sebacic acid) (PEG-PSA) (Tang et al., 2010) have been developed for lung cancer treatment applications, the introduction of foreign matter to the lung has the potential to induce complications. In this work, a first-line lung cancer chemotherapeutic drug, paclitaxel (PTX), was encapsulated in a PEGylated phospholipid microparticle/nanoparticle system comprised of dipalmitoylphosphatidylcholine (DPPC) and dipalmitoylphosphatidylethanolamine-methoxy(polyethylene glycol) (DPPE-PEG). DPPC was chosen as the main excipient because it is the primary phospholipid component in lung surfactant (Mansour et al., 2011). In addition to

offering a natural excipient component to the formulated particles, the use of phospholipids as biocompatible biodegradable excipients can aid in the delivery of drugs to the lungs as they have been shown to improve particle migration to the lung periphery due to the reduction in surface tension provided by the surfactant (Ganguly et al., 2008; Mansour et al., 2001; Mansour and Zografi, 2007a, b). The use of PEGylated phospholipids, such as DPPE-PEG, can result in a formulation that could evade recognition and uptake of the immune system allowing for prolonged residence time in the lung (Ishihara et al., 1998; Labiris and Dolovich, 2003a, b; Mansour et al., 2011; Mansour et al., 2010), have mucopenetrating properties (Lai et al., 2009a; Lai et al., 2009b), and are used in marketed intravenous (IV) nanopharmaceutical products (Mansour et al., 2011; Mansour et al., 2010; Rhee and Mansour, 2011; Wu and Mansour, 2011). Also, for certain formulations, the relatively low clearance rate in the bronchioalveolar region may also allow for longer residence times (Carvalho et al., 2011). We have recently reported on the successful design and optimization of the novel DPI nanomedicine carrier platform consisting of DPPC/DPPE-PEG with varying PEG chain length and excellent aerosol dispersion performance as aerosolized dry powders (Meenach et al., 2012b).

Paclitaxel was chosen for this study since it is one of the most widely used drugs to treat lung cancer and is a first-line drug in the treatment of lung cancer (Carvalho et al., 2011; Eldar-Boock et al., 2011). Taxol®, the intravenous formulation of paclitaxel contains water-insoluble paclitaxel along with a mixture of Cremophor EL and dehydrated ethanol, and has been shown to cause adverse reactions such as hypersensitivity, muscle pain, and neurologic and cardiac toxicities (Marupudi et al., 2007). Paclitaxel is lipophilic, with high protein affinity, and also exhibits a volume of distribution much higher than the total water volume in the body, which causes it to have a low therapeutic index (Carvalho et al., 2011). The low solubility of paclitaxel

140 in water (0.7 to 30 μg/ml) (Liggins et al., 1997) can be overcome via encapsulation into a solid-
141 state particle system helping to overcome this major hurdle.

142 The objective of this systematic study was to rationally develop and characterize an
143 inhalable PEGylated phospholipid microparticulate/nanoparticulate dry powder aerosol platform
144 containing paclitaxel with varying PEG chain lengths and paclitaxel content for the treatment of
145 lung cancer. The organic solution advanced co-spray dried (co-SD) paclitaxel/PEGylated
146 phospholipid dry powder inhalation aerosol microparticulate/nanoparticulate formulations were
147 compared to one-component systems of spray dried paclitaxel. The formulated particles
148 contained a fixed amount of DPPC to DPPE-PEG with varying PEG chain lengths of 2k, 3k, and
149 5k and with varying paclitaxel ratios (5, 25, 50, and 75 mole % of paclitaxel overall). To the
150 authors' knowledge, this is the first time to report on a comprehensive and systematic study on
151 this novel anticancer lipopolymeric dry powder inhalation aerosol formulation platform
152 engineered from organic solution advanced spray drying (i.e. no water) consisting of
153 microparticles and nanoparticles of DPPC and DPPE-PEG with varying PEG chain lengths with
154 various combinations of PTX for pulmonary chemotherapeutic delivery in lung cancer.
155

156 **2.1 MATERIALS AND METHODS**

157 **2.1.1 Materials**

158 Synthetic dipalmitoylphosphatidylcholine (DPPC, Molecular Weight: 734.039 g/mol; >99%
159 purity) and dipalmitoylphosphatidylethanolamine-methoxy(polyethylene glycol) (DPPE-PEG,
160 Molecular Weights: 2749.391 g/mol, 3716.304 g/mol, and 5741.510 g/mol which correspond to
161 2000, 3000 and 5000 molecular weight poly(ethylene glycol) lengths per compound; >99%
162 purity) were obtained from Avanti Polar Lipids (Alabaster, AL, USA). Paclitaxel was obtained
163 from LC Labs (Woburn, MA, USA; 99.5% purity; $C_{47}H_{51}NO_{14}\cdot H_2O$). Methanol (HPLC grade,

ACS certified) and chloroform (HPLC grade, ACS certified) were obtained from Fisher Scientific (Pittsburg, PA, USA). HYDRANAL$^{@}$-Coulomat AD was from Sigma-Aldrich (St. Louis, MO, USA). Ultra-high purity (UHP) dry nitrogen gas was from Scott-Gross (Lexington, KY, USA). All materials were used as received and stored at -20°C.

### 2.1.2 Spray-Drying and Co-Spray Drying from Dilute Drug Feed Solution

Advanced spray-drying of co-spray dried (co-SD) paclitaxel-loaded PEGylated phospholipid particles was performed using a B-290 Büchi Mini Spray Dryer coupled with a B-295 Inert Loop and high performance cyclone (all from Büchi Labortechnik AG, Switzerland) in closed-mode using UHP dry nitrogen as the atomizing gas. The nozzle diameter (composed of stainless steel) was 0.7 mm and the spray-drying (SD) particles were separated from the drying gas (using UHP dry nitrogen) in the high-performance cyclone and collected in a sample collector. The feed solutions were prepared by dissolving DPPC and DPPE-PEG (i.e. 95 mole % DPPC to 5 mole % DPPE-PEG) with different amounts of paclitaxel (PTX) ranging from 5 to 75 mole% paclitaxel to total DPPC/DPPE-PEG in methanol to form dilute concentration feed solutions of 0.1% w/v. Based on our previous work (Li et al., 2011; Li and Mansour, 2011; Meenach et al., 2012b), the following spray-drying conditions were used: atomization gas flow rate of 600 L/h, aspiration rate of 35 $m^3$/h, inlet temperature of 150 °C (which represents the primary drying step), and pump rate of 30 mL/min (High P). Table I shows the various formulated particle systems and their corresponding PTX and DPPC/DPPE-PEG amounts and types and outlet temperatures (which represent the secondary drying process temperatures). For pure spray dried (SD) paclitaxel particles, the same atomization gas flow rate, aspiration rate, and inlet temperatures were used as for the PEGylated phospholipid systems. The pump rate was varied at 3 mL/min

187 (Low P), 15 mL/min (Med P), and 30 mL/min (High P). All SD and co-SD powders were stored
188 in glass vials sealed with parafilm in desiccators over indicated Drierite™ desiccant at -23°C
189 under ambient pressure.
190
191 **2.1.3 Scanning Electron Microscopy (SEM) for Morphology and Shape Analysis**
192 The shape and surface morphology of particles was evaluated by SEM, using a Hitachi S-4300
193 microscope (Tokyo, Japan). Samples were placed on double-sided adhesive carbon tabs and were
194 adhered to aluminum stubs (TedPella, Inc., Redding, CA, USA) which were coated with a
195 gold/palladium alloy thin film using an Emscope SC400 sputter coating system at 20 μA for 1
196 minute under Argon gas. The electron beam with an accelerating voltage of 5 - 10 kV was used
197 at a working distance of 13.3 – 15.3 mm. Images were captured at several magnifications using
198 similar conditions previously reported by the authors.(Meenach et al., 2012b)
199
200 **2.1.4 Particle Sizing and Size Distribution**
201 The mean size, standard deviation, and size range of the particles were determined digitally using
202 SigmaScan™ 5.0 software (Systat, San Jose, CA, USA), as previously reported by the
203 authors.(Meenach et al., 2012b) Representative micrographs for each particle sample at 5,000x
204 magnification were analyzed by measuring the diameter of at least 100 particles per image.
205
206 **2.1.5 Karl Fisher (KF) Coulometric Titration**
207 The water content of all particle powders was chemically quantified by Karl Fisher (KF)
208 coulometric titration, using similar conditions previously reported by the authors.(Li and
209 Mansour, 2011; Meenach et al., 2012b) The measurements were performed with a 737 KF

Coulometer coupled with 703 Ti Stand (Metrohm Ltd., Antwerp, Belgium). Approximately 5 mg of powder was dissolved in a known volume of chloroform. The sample solution was injected into the reaction cell that contained HYDRANAL® KF reagent and the water content was then calculated from the resulting reading.

### 2.1.6 Differential Scanning Calorimetry (DSC)

Thermal analysis and phase transition measurements were carried out using a TA Q200 DSC system (TA Instruments, New Castle, DE, USA) equipped with T-Zero® technology and an automated computer-controlled RSC-90 cooling accessory. Using similar conditions previously reported by the authors,(Li and Mansour, 2011; Meenach et al., 2012b) 1 - 3 mg of powder was weighed into hermetic anodized aluminum T-Zero® DSC pans and were sealed hermetically sealed with the T-Zero® hermetic sealer. UHP dry nitrogen gas was used as the purging gas at 50 mL/min. The heating range was 0 – 250 °C at a heating scan rate of 5.00 °C/min.

### 2.1.7 Powder X-ray Diffraction (XRPD)

XRPD patterns of powder samples were measured by a Rigaku Multiflex X-ray diffractometer (The Woodlands, TX, USA) with a slit-detector Cu Kα radiation source (40 kV, 44 mA, and $\lambda$ = 1.5406 Å). The scan range was 5 – 50° in 2θ with a scan rate of 2°/min at ambient temperature. The sample was placed on a horizontal quartz glass sample holder plate.

### 2.1.8 Attenuated Total Reflectance-Fourier Transform Infrared Spectroscopy (ATR-FTIR)

ATR-FTIR was performed using a Varian Inc. 7000e step-scan spectrometer (Agilent Technologies, Santa Clara, CA, USA). The particle powder was placed on the diamond ATR

crystal, covered with a glass cover slip, and held in place with a specialized clamp. ATR crystal and IR spectra were obtained at an 8 $cm^{-1}$ spectral resolution between 700 and 4000 $cm^{-1}$. The data was collected and analyzed using Varian Resolutions software.

### 2.1.9 Hot-Stage Microscopy (HSM)

HSM studies were completed using an Olympus BX51 polarized microscope (Olympus, Japan) equipped with an Instec STC200 heating unit and S302 hot stage (Boulder, CO, USA). The polarized light was filtered by a γ 530 nm U-TP530 filter lens. Powder samples were mounted on a cover glass and heated from 25 °C to 250 °C at a heating rate of 5 °C/min. The heating program was controlled by WinTemp software and images were digitally captured via a SPOT Insight digital camera (Diagnostic Instruments, Inc., Sterling Heights, MI, USA).

### 2.1.10 Paclitaxel Loading Analysis via UV-Vis Spectroscopy

UV-Vis was used to determine the amount of paclitaxel loaded into the formulated particle systems. The particles were dissolved in known quantities of methanol prior to analysis. The absorbance intensity was measured at 227 nm using a UV-1800 UV-Vis Shimadzu spectrophotometer and a calibration curve of paclitaxel in methanol was used. The paclitaxel encapsulation efficiency (EE) and loading was calculated as follows:

$$\text{Encapsulation Efficiency (EE)} = \frac{Actual\ Mass\ of\ PTX}{Initial\ Mass\ of\ PTX}\ x\ 100\%$$

$$\text{Drug Loading} = \frac{Actual\ Mass\ of\ PTX}{Mass\ of\ Particles}$$

256 **2.1.11 *In Vitro* Aerosol Dispersion Performance via Next Generation Impactor™ (NGI™)**

257 In accordance with United States Pharmacopeia (USP) Chapter <601> specifications on aerosols
258 (2006) the *in vitro* aerosol dispersion properties of the dry powder particles were determined
259 using the Next Generation Impactor™ (NGI™) with a stainless steel induction port (i.e. USP
260 throat) attachment (NGI™ Model 170, MSP Corporation, Shoreview, MN, USA), equipped with
261 specialized stainless steel NGI™ gravimetric insert cups (MSP Corporation, Shoreview, MN,
262 USA). The NGI™ was coupled with a Copley TPK 2000 critical flow controller, which was
263 connected to a Copley HCP5 vacuum pump (Copley Scientific, United Kingdom). The airflow
264 rate, Q, was measured and adjusted prior to each experiment using a Copley DFM 2000 flow
265 meter (Copley Scientific, United Kingdom).

266 The aerosolization studies were experimentally designed by Design Expert™ 8.0.7.1
267 software (Stat-Ease Corp., MN, USA). Glass fiber filters (55 mm, Type A/E, Pall Life Sciences,
268 Exton, PA, USA) were placed in the stainless steel NGI™ gravimetric insert cups for NGI™
269 stages 1 through 7 to minimize bounce or re-entrapment (Edwards et al., 1998). Three
270 hydroxypropyl methylcellulose hard capsules (size 3, Quali-V®, Qualicaps® Inc., Whitsett, NC,
271 USA) were each loaded with 10 mg of powder which were then loaded into a high resistance (i.e.
272 high sheer stress) FDA-approved human DPI device, the Handihaler® (Boehringer Ingelheim &
273 Pfizer Ltd., USA), and tightly inserted into the induction port. The NGI™ was run at a controlled
274 flow rate (Q) at 60 L/minute with a delay time of 10 seconds (NGI™ Flow controller) prior to
275 the capsules being needle-pierced open by the Handihaler® mechanism, where the particles were
276 then drawn into the impactor for 10 seconds. This was done with a total of 3 capsules per sample
277 for a total of 30 mg total per run. For each 30 mg run, the amount of particles deposited onto
278 each stage was determined gravimetrically by measuring the difference in mass of the glass

filters after particle deposition. For the NGI™ flow rate of 60 L/minute, the effective cutoff diameters for each impaction stage were calibrated by the manufacturer and stated as: Stage 1 (8.06 μm); Stage 2 (4.46 μm); Stage 3 (2.82 μm); Stage 4 (1.66 μm); Stage 5 (0.94 μm); Stage 6 (0.55 μm); and Stage 7 (0.34 μm). The fine particle dose (FPD), fine particle fraction (FPF), respirable fraction (RF), and emitted dose (ED) were calculated as follows:

Fine particle dose (FPD) = mass of particles < 4.4 μm (Stages 2 through 7)

$$\text{Fine particle fraction (FPF)} = \frac{\text{fine particle dose}}{\text{initial particle mass loaded into capsules}} \text{ x } 100\%$$

$$\text{Respirable fraction (RF)} = \frac{\text{mass of particles} < 4.4\ \mu\text{m (Stages 2 through 7)}}{\text{total particle mass on all stages}} \text{ x } 100\ \%$$

$$\text{Emitted dose (ED)} = \frac{\text{initial mass in capsules} - \text{final mass remaining in capsules}}{\text{initial mass in capsules}}\ x\ 100\ \%$$

The mass mean aerodynamic diameter (MMAD) and geometric standard deviation (GSD) were determined using a Mathematic program written by Dr. Warren Finlay.(Finlay, 2008) All experiments were triplicated (n = 3).

### 2.1.12 Statistical Analysis

All experiments were performed in at least triplicate. The aerosolization studies were experimentally designed by Design Expert™ 8.0.7.1 software (Stat-Ease Corp., MN, USA). MYSTAT 12 for Windows (12.01.00) was used for t-tests (paired t-test with unequal variances)

to determine any significance in observed data. A p-value of $< 0.05$ was considered statistically significant.

## 3.1 RESULTS AND DISCUSSION

### 3.1.1 SEM, Particle Sizing, and Size Distribution

Formulated particle and surface morphologies were visualized and analyzed via SEM micrographs as seen in Figures 1 through 5. Their corresponding diameters are exhibited in Table I as determined via SigmaScan™ software. 5PTX:95DPPC, 5PTX:95DPPC/DPPE-PEG2k, and 5PTX:95DPPC/DPPE-PEG3k particles were smooth and spherical whereas 5PTX:95DPPC:DPPE-PEG5k demonstrated characteristics of sintering between the particles. 25PTX:75DPPC and 25PTX:75DPPC/DPPE-PEG2k were also smooth and spherical whereas 25PTX:75DPPC/DPPE-PEG3k and 25PTX:75DPPC/DPPE-PEG5k demonstrated characteristics of sintering between the particles. The 50PTX and 75PTX systems (Figures 3 and 4, respectively) demonstrated an increase in corregation as seen in Figure 5. This phenomenon was seen in our previous systems comprised of pure SD PTX (Meenach et al., 2012b). As the amount of PTX in the particle systems increased, the degree of sintering and corregation of the particles also increased. The sintering for the particles with high PEG content is likely due to the low glass transition temperature for PEG, which is around -60°C (Törmälä, 1974). The diameter of all formulated dry powder systems ranged from 0.624 to 3.416 μm in diameter and there was a slight decrease in size with increasing amounts of paclitaxel, although this was not significant. There were no changes in the diameter due to the degree of PEGylation from DPPE-PEG. Overall, the particles were within the ideal size range necessary for inhalation into the deep lung

for both adults and children (Bosquillon et al., 2001; Coates and O'Callaghan, 2006) which is necessary for effective pulmonary delivery for treating lung cancer.

### 3.1.2 Karl Fisher (KF) Coulometric Titration

The residual water content of the formulated particles in the solid-state are shown in Table I. The water content for the co-SD formulated particles ranged from 1.47 % to 6.78 % (w/w) with no trends corresponding to excipient formulation or amount of paclitaxel present in the system. The pure SD PTX particles exhibited the lowest water content ranging from 0.44 % to 2.47 % (w/w). These values were slightly higher than those reported for the raw components (Meenach et al., 2012b), however, all of the values were low and well within the range previously reported by our group in other inhalable dry powder formulations. Low water content is a requirement for efficient dry powder aerosolization and effective particle delivery since water can significantly decrease the dispersion properties of dry powders during aerosolization due to the interparticulate capillary forces acting at the solid-solid interface between particles (Hickey et al., 2007a).

### 3.1.3 Differential Scanning Calorimetry (DSC)

As seen in Figure 6a for the 5PTX particles, an endothermic main phase transition peak ($T_c$) was observed between 63°C and 65°C for all samples which corresponds to the gel-to-liquid self-assembly phase transition of raw DPPC, where the hydrophobic acyl chain core melts, indicating the presence of the phospholipid bilayer structure (Mansour and Zografi, 2007a, b; Pappalardo et al., 2005). The co-SD 5PTX samples with PEG3k and PEG5k also exhibited endothermic peaks at 41.5°C and 47.2°C, respectively, which corresponds to the presence of DPPE-PEG. These two

endothermic peaks are also present in raw DPPC and DPPE-PEG as we have shown previously (Meenach et al., 2012b). The enthalpy values for the 5PTX particles ranged from 22.1 to 25.7 J/g but there was no correlation due to the excipient used. 25PTX samples (Figure 6b) also exhibited strong transition peaks between 63°C and 66°C and 25PTX:DPPC/DPPE-PEG5k particles showed peaks near 45°C and 47°C. The enthalpy values for the 25PTX particles ranged from 13.1 to 20.7 J/g but there was no correlation due to the excipient used. Both 5PTX and 25PTX systems underwent a metastable phase transition around 145°C which is likely the result of reorganization of the molecules within the particles. For the 50PTX formulated particles (Figure 6c) there were no measurable transition peaks with the exception of 50PTX:50DPPC/DPPE-PEG5k, which exhibited small peaks at 49.2°C and 65.54°C with corresponding enthalpies of 3.045 and 0.938 J/g. These correspond to the DPPC and DPPE-PEG bilayer phase transitions, respectively. In Figure 6d, the 75PTX samples indicate no measurable transition peaks in the phospholipid region (40°C to 70°C) but did exhibit a large exothermic peak around 212°C which corresponds to the degradation of the sample (also seen in panel e for raw PTX. The size of these peaks, and corresponding enthalpies, decrease with increasing PEG content at 88.4, 71.4, 59.0, and 15.9 J/g for DPPC, PEG2k, PEG3k, and PEG5k samples, respectively. Furthermore, the 75PTX formulations exhibited a glass transition temperature ($T_g$) near 146°C, which is a second-order phase transition for the amorphous glass-to-rubbery state as seen in Figure 6f. Raw PTX exhibited a small endothermic peak around 204°C which corresponds to the melting temperature ($T_m$) of paclitaxel, which is a first-order phase transition whereas no measurable melting peaks were seen prior to degradation for SD samples. Both the $T_g$ and $T_m$ values were similar to those demonstrated by the spray dried and raw paclitaxel formulations as seen in Figure 6e and compares to what has previously been shown for raw paclitaxel (Lee et al., 2001; Liggins et al.,

1997). Overall, the limited presence of transition peaks from 40 to 70°C for both 50PTX and 75PTX particles indicate limited multilamellar formation of the phospholipids within the particle matrix.

### 3.1.4 X-ray Diffraction (XRPD)

X-ray powder diffractograms (Figure 7) showed the a strong peak at 21° 2Θ for all SD 5PTX and SD 25PTX formulated particles which corresponds to the presence of the solid-state phospholipid bilayer structure (Alves and Santana, 2004) indicating that the bilayer structure is preserved in the solid-state following organic solution advanced spray drying in closed-mode. These samples also exhibited strong peaks at 19 and 23° 2Θ which designate the metastable phase of PEG as seen in previous results for PEG powders (Kang et al., 2007). The intensity of the 19 and 23° 2Θ peaks increased with increasing PEG chain length for the SD 5PTX and SD 25PTX systems. The intensities of the 19 and 23° 2Θ peaks for the co-SD systems are lower overall in comparison to that seen for raw DPPC or DPPE-PEG (Meenach et al., 2012b). For the SD 50PTX and SD 75PTX formulated particles no strong peaks were present, indicating that PTX is amorphous within the particle matrix, likely with limited bilayer formation within the particles. The lack of characteristic peaks likely indicates that there is no detectable phospholipid bilayer structure for these powder systems within the detection limit of XRPD. The intensities of the peak corresponding to 21°C 2Θ decreased with increasing paclitaxel content. Raw paclitaxel showed peaks throughout its diffractograms indicating its crystallinity prior to spray drying.

### 3.1.5 Attenuated Total Reflectance Fourier Transform Infrared Spectroscopy (ATR-FTIR)

Formulated particles and their raw counterparts underwent ATR-FTIR analysis to determine the functional groups present in the systems (Figure 8). For both the raw DPPC and raw DPPE-PEG powders, the spectra indicated the same characteristic peaks as previously reported in literature for DPPC and PEG, respectively (Lee et al., 2001; Meenach et al., 2012b). The formulated co-SD PTX:DPPC/DPPE-PEG3k particles exhibited sharp peaks at 2916 $cm^{-1}$ ($-CH_2-$ antisymmetrical stretching), 2870 $cm^{-1}$ ($-CH_2-$ symmetrical stretching), 1724 $cm^{-1}$ (C=O ester stretching), 1465 $cm^{-1}$ ($-CH_2-$ deformation), 1060 $cm^{-1}$ (-C-C-), and 965 $cm^{-1}$ (($-N^+(CH_3)_3$ antisymmetrical stretching) which all increased with increasing paclitaxel content. These peaks were present in both raw DPPC and DPPE-PEG3k but not raw or formulated paclitaxel. For the peak at 1724 $cm^{-1}$, it was split for the raw PTX but not for the spray dried particles. Overall, ATR-FTIR analysis of the solid-state particles confirmed the presence of DPPC and DPPE-PEG where appropriate through the signature peaks of each component and the difference between SD paclitaxel and raw paclitaxel was confirmed by differing spectra between the two systems.

### 3.1.6 Cross-Polarizing Light Hot-Stage Microscopy (HSM)

Representative micrographs of co-SD 5PTX:95DPPC/DPPE-PEG3k and co-SD 50PTX:50DPPC/DPPE-PEG3k are shown in Figure 9. The co-SD 5PTX:95DPPC/DPPE-PEG3k formulated particles showed dark agglomerates that lack birefringency between 25°C and 60°C, which indicated a non-ordered, amorphous material. A phase transition was visualized near 65°C, which likely corresponds to the gel-to-liquid self-assembly bilayer main phase transition as shown in the DSC thermogram at 65°C in Figure 6a. Melting was visualized starting at 120°C with the formation of liquid droplets with decomposition occurring at 250°C. The micrographs for co-SD 50PTX:50DPPC/DPPE-PEG3k showed large agglomerates lacking birefringency

between 25°C and 80°C and a visible phase transition began starting around 90°C as shown by deformation of the particles. Melting started around 150°C and was complete by 155°C and decomposition occurred by 225°C. Pure SD paclitaxel (100PTX) showed dark agglomerates that lack birefringency between 25°C and 170°C. The particles began melting around 180°C as seen in Figure 10a. Raw paclitaxel had dark agglomerates lacking birefringency from 25°C to 180°C. Once the paclitaxel began melting at 190°C, it exhibited birefringency until decomposition around 240°C. Overall, HSM confirmed the amorphous nature of the formulated co-SD PTX:DPPC/DPPE-PEG systems as well as for SD 100PTX particles as no birefringency was observed. It also demonstrated the stability of the particles at room and physiological temperatures.

### 3.1.7 Paclitaxel Loading

Paclitaxel loading into the PEGylated phospholipid dry powder particles was determined by dissolving them in methanol and measuring the concentration of drug via UV-Vis spectroscopy. As shown in Table I, the PTX encapsulation efficiencies for 5PTX systems was the highest (ranging from 94.7% to 99.0%) and decreased with increasing PTX content. As expected, the paclitaxel loading increased with increasing PTX content where the SD 5PTX, 25PTX, 50PTX and 75PTX systems exhibited values in the range of 41.3 - 60.2 μg/mg, 191.4 - 242.6 μg/mg, 316.8 - 511.0 μg/mg, and 571.2 - 679.9 μg/mg, respectively. Furthermore, the encapsulation values for the 25 – 75% PTX-loaded particles is high enough for the dose necessary for animal treatment. In particular, systems containing 100 – 500 μg/mg PTX contain enough paclitaxel to result in a dose to rats ranging from 2 – 4 mg/kg at 2 – 5 mg particles/rat, which has been

436 demonstrated as an effective dose range in the treatment of an orthotopic lung cancer model (Gill
437 et al., 2011; Yang et al., 2007).
438
439 **3.1.8 *In Vitro* Aerosol Dispersion Performance via Next Generation Impactor™**
440 The aerosol dispersion properties of the co-SD particles and pure PTX SD particles were
441 evaluated using the Next Generation Impactor™ (NGI™) coupled with a Handihaler® DPI
442 device. As seen in Table II, the MMAD values for co-SD systems (regardless of PTX loading)
443 increased with increasing PEG chain length and decreased with increasing PTX loading. The
444 corresponding GSD also increased with increasing PEG chain length. Furthermore, for 100PTX
445 particles, the MMAD values were approximately the same (ranging from 3.2 μm to 3.4 μm)
446 whereas the GSD values were 2.3 μm to 2.6 μm. In general, fine particle fractions (FPF) and
447 respirable fractions (RF) decreased with increasing PEG content, while the emitted dose (ED)
448 increased. There was no discernible difference for FPF, RF, and ED with respect to the PTX
449 loading. Figure 11 shows the aerosol dispersion performance of the dry powders as the %
450 deposition on each NGI™ stage for both the co-SD and pure PTX systems. Aerosol deposition
451 on each NGI™ stage is measurable and in particular, deposition on the lower stages of stage 2 all
452 the way to stage 7 (lowest stage) is observed. In general, the % deposition on stage 1 increased
453 with increasing PEG chain length. The exception to this was seen for the SD 50PTX dry powder
454 aerosols where no difference was seen due to PEG chain length. This trend was opposite for
455 stage 4 where the amount of powder deposited on this stage decreased with increasing PEG
456 content for co-SD particles. For 100PTX SD dry powder aerosol, there was no difference
457 between the amounts of powder deposited on each stage. In regards to paclitaxel loading, the
458 amount of powder deposited on each stage decreased slightly with increasing PTX content. Since

459 there was significant particle deposition on Stages 5 – 7 (where the MMAD for these particular
460 particles would be less than 1 μm), the particles on these stages should deposit in the lower
461 airways of the lungs due to diffusion of the particles into this region via Brownian motion
462 (Suarez and Hickey, 2000). Overall, the particles exhibit characteristics that will allow them to
463 deposit in nearly all regions of the lung allowing for treatment throughout the entirety of the
464 tissue.

465 The MMAD values for most of the particle systems were within the range necessary (1 –
466 10 μm) for particles to deposit predominantly in the middle-to-deep lung regions and deposit by
467 sedimentation due to gravitational settling (Carvalho et al., 2011; Edwards, 1995a, b; Hickey and
468 Mansour, 2008; Hickey and Mansour, 2009; Suarez and Hickey, 2000). Furthermore, the ED
469 values of co-SD particles remained approximately the same compared to systems without PTX
470 (Meenach et al., 2012b). The RF values for the co-SD systems are lower than their corresponding
471 drug-free systems reported by our group (45-50% compared to 60-70%) (Meenach et al., 2012b).
472 While the RF values of the co-SD powders were lower than their respective values at a given
473 PEG chain length for the PTX-free powders, their respective FPF values increased significantly
474 (43-79% compared to 20-30%) (Meenach et al., 2012b).
475

476 **4.1 CONCLUSIONS**

477 This systematic and comprehensive study demonstrated for the first time that organic solution
478 advanced spray drying and co-spray drying in closed-mode of a dilute concentration feed
479 solution can be successfully employed to formulate high performing DPI liposphere aerosols
480 consisting of co-spray dried paclitaxel (a first-line chemotherapeutic lung cancer drug) into a
481 biocompatible and biodegradable lipopolymeric system (DPPE-PEG) with varying PEG chain

length and containing the essential lung surfactant phospholipid, DPPC. The physicochemical characterization of these particles indicates that they would be suitable to deliver PTX to the middle and deep regions of the lungs to deliver the drug in a targeted fashion. For multilamellar particles, a lower paclitaxel loading will likely be optimal along with a medium PEGylation (using DPPE-PEG3k). The incorporation of DPPE-PEG lipopolymer of varying PEG chain length can potentially offer enhanced mucus penetration by phospholipid spreading and PEG penetration, controlled drug release, and "stealth" property of evasion of phagocytosis by immune cells.

## 5.1 ACKNOWLEDGEMENTS

The authors gratefully acknowledge financial support from the National Cancer Institute (NCI) Grant Number R25CA153954 and a National Cancer Institute Cancer Nanotechnology Training Center (NCI-CNTC) Postdoctoral Traineeship awarded to SAM. The content is solely the responsibility of the authors and does not necessarily represent the official views of the National Cancer Institute or the National Institutes of Health. The authors thank Dr. Tonglei Li for XRPD and HSM access and Dr. J. Zach Hilt for ATR-FTIR access.

## AUTHOR DISCLOSURE STATEMENT

No conflicts of interest exist.

## REFERENCES


2006. <601> Aerosols, Nasal Sprays, Metered-Dose Inhalers, and Dry Powder Inhalers Monograph, USP 29-NF 24 The United States Pharmacopoeia and The National Formulary: The Official Compendia of Standards. The United States Pharmacopeial Convention, Inc., Rockville, MD, pp. 2617-2636.

Alves, G.P., Santana, M.H.A., 2004. Phospholipid dry powders produced by spray drying processing: structural, thermodynamic and physical properties. Powder Technology 145, 139-148.

Arnold, M.M., Gonnan, E.M., Schieber, L.J., Munson, E.J., Berkland, C., 2007. NanoCipro encapsulation in monodisperse large porous PLGA microparticles. Journal of Controlled Release 121, 100-109.

Bosquillon, C., Lombry, C., Preat, V., Vanbever, R., 2001. Influence of formulation excipients and physical characterisitcs of inhalation dry powders on their aerosolization performance. Journal of Controlled Release 70, 329-339.

Cartiera, M.S., Ferreira, E.C., Caputo, C., Egan, M.E., Caplan, M.J., Saltzman, W.M., 2010. Partial Correction of Cystic Fibrosis Defects with PLGA Nanoparticles Encapsulating Curcumin. Molecular Pharmaceutics 7, 86-93.

Carvalho, T.C., Carbalho, S.R., McConville, J.T., 2011. Formulations for pulmonary administration of anticancer agents to treat lung malignancies. Journal of Aerosol Medicine and Pulmonary Drug Delivery 24, 61-80.

Chow, A.H.L., Tong, H.H.Y., Chattopadhyay, P., Shekunov, B.Y., 2007. Particle engineering for pulmonary drug delivery. Pharmaceutical Research 24, 411-437.

Coates, A.L., O'Callaghan, C., 2006. Drug administration by aerosol in children. Saunders-Elsevier, Philadelphia, PA.

Edwards, D.A., 1995a. THE MACROTRANSPORT OF AEROSOL-PARTICLES IN THE LUNG - AEROSOL DEPOSITION PHENOMENA. Journal of Aerosol Science 26, 293-317.

Edwards, D.A., 1995b. The macrotransport of aerosol particles in the lung: Aerosol deposition phenomena. Journal of Aerosol Science 26, 293-317.

Edwards, D.A., Ben-Jebria, A., Langer, R., 1998. Recent advances in pulmonary drug delivery using large, porous inhaled particles. Journal of Applied Physiology 85, 379-385.

Eldar-Boock, A., Miller, K., Sanchis, J., Lupu, R., Vicent, M.J., Satchi-Fainaro, R., 2011. Integrin-assisted drug delivery of nano-scaled polymer therapeutics bearing paclitaxel. Biomaterials 32, 3862-3874.

Finlay, W., 2008. The ARLA Respiratory Deposition Calculator.

Gagnadoux, F., Hureaux, J., Vecellio, L., Urban, T., Le Pape, A., Valo, I., Montharu, J., Leblond, V., Boisdron-Celle, M., Lerondel, S., Majoral, C., Diot, P., Racineux, J.L., Lemarie, E., 2008. Aerosolized chemotherapy. Journal of Aerosol Medicine and Pulmonary Drug Delivery 21, 61-69.

Ganguly, S., Moolchandani, V., Roche, J.A., Shapiro, P.S., Somaraju, S., Eddington, N.D., Dalby, R.N., 2008. Phospholipid-induced in vivo particle migration to enhance pulmonary deposition. Journal of Aerosol Medicine Pulmonary Drug Delivery 23, 181-187.

Gilani, K., Najafabadi, A.R., Barghi, M., Rafiee-Tehrani, M., 2005. The effect of water to ethanol feed ratio on physical properties and aerosolization behavior of spray dried cromolyn sodium particles. Journal of Pharmaceutical Sciences 94, 1048-1059.

547 Gill, K.K., Nazzal, S., Kaddoumi, A., 2011. Paclitaxel-loaded PEG5000-DSPE micelles as
548 pulmonary delivery platform: Formulation characterizaton, tissue distribution, plasma
549 pharmacokinetics and toxicological evaluation. European Journal of Pharmaceutics and
550 Biopharmaceutics 79, 276-284.
551 Gill, S., Lobenberg, R., Ku, T., Azarmi, S., Roa, W.H., Prenner, E.J., 2007. Nanoparticles:
552 characteristics, mechanisms of action, and toxicity in pulmonary drug delivery - a review.
553 Journal of Biomedical Nanotechnology 3, 107-119.
554 Hayes, D., Ball, A.M., Mansour, H.M., Martin, C.A., Flynn, J.D., 2011. Fungal Infection in
555 Heart-Lung Transplant Recipients Receiving Single-agent Prophylaxis with Itraconazole.
556 Experimental and Clinical Transplantation 9, 399-404.
557 Hickey, A.J., Mansour, H.M., 2008. Formulation Challenges of Powders for the Delivery of
558 Small Molecular Weight Molecules as Aerosoles, in: Rathbone, M.J., Roberts, M.S., Lane, M.E.
559 (Eds.), Modified-Release Drug Delivery Technology Informa Healthcare, New York, pp. 573-
560 602.
561 Hickey, A.J., Mansour, H.M., 2009. Delivery of drugs by the pulmonary route, in: Florence,
562 A.T., Siepmann, J. (Eds.), Modern Pharmaceutics, 5th ed. Taylor and Francis, New York, pp.
563 191-219.
564 Hickey, A.J., Mansour, H.M., Martin, J.T., Xu, Z., Smyth, H.D.C., Mulder, T., McLean, R.,
565 Langridge, J., Papadopoulos, D., 2007a. Physical Characterization of Component Particles
566 Included in Dry Powder Inhalers. I. Strategy Review and Static Characteristics. Journal of
567 Pharmaceutical Sciences 96, 1282-1301.
568 Hickey, A.J., Mansour, H.M., Telko, M.J., Xu, Z., Smyth, H.D.C., Mulder, T., McLean, R.,
569 Langridge, J., Papadopoulos, D., 2007b. Physical characterization of component particles
570 included in dry powder inhalers. II. Dynamic characteristics. Journal of Pharmaceutical Sciences
571 96, 1302-1319.
572 Ishihara, K., Nomura, H., Mihara, T., Kurita, K., Iwasaki, Y., Nakabayashi, N., 1998. Why do
573 phospholipid polymers reduce protein adsorption? Journal of Biomedical Materials Research 39,
574 323-330.
575 Kang, E., Robinson, J., Park, K., Cheng, J.-X., 2007. Paclitaxel distribution in poly(ethylene
576 glycol)/poly(lactide-co-glycolic acid) blends and its release visualized by coherent anti-Stokes
577 Raman scattering microscopy. Journal of Controlled Release 122, 261-268.
578 Kikuchi, H., Yamauchi, H., Hirota, S., 1991. A spray-drying method for mass production of
579 liposomes. Chemical & Pharmaceutical Bulletin 36, 1522-1527.
580 Labiris, N.R., Dolovich, M.B., 2003a. Pulmonary drug delivery. Part I: Physiological factors
581 affecting therapeutic effectiveness of aerosolized medications. Journal of Clinical Pharmacology
582 56, 588-599.
583 Labiris, N.R., Dolovich, M.B., 2003b. Pulmonary drug delivery. Part II: The role of inhalant
584 delivery devices and drug formulation in therapeutic effectiveness of aerosolized medications.
585 British Journal of Clinical Pharmacology 56, 600-612.
586 Lai, S.K., Wang, Y.-Y., Hanes, J., 2009a. Mucus-penetrating nanoparticles for drug and gene
587 delivery to mucosal tissues. Advanced Drug Delivery Reviews 61, 158-171.
588 Lai, S.K., Wang, Y.-Y., Wirtz, D., Hanes, J., 2009b. Micro- and macrorheology of mucus.
589 Advanced Drug Delivery Reviews 61, 86-100.
590 Lee, J.H., Gi, U.-S., Kim, J.-H., Kim, Y., Kim, S.-H., Oh, H., Min, B., 2001. Preparation and
591 Characterization of Solvent Induced Dihydrated, Anhydrous, and Amorphous Paclitaxel. Bulletin
592 of the Korean Chemical Society 22, 925-928.

593 Li, X., Hayes, D., Mansour, H.M., 2011. Targeted lung delivery by inhalable multifunctional
594 microparticulate/nanoparticulate aerosols for cystic fibrosis combination drug/mucolytic
595 treatment. Pediatric Pulmonology, 346-346.
596 Li, X.J., Mansour, H.M., 2011. Physicochemical Characterization and Water Vapor Sorption of
597 Organic Solution Advanced Spray-Dried Inhalable Trehalose Microparticles and Nanoparticles
598 for Targeted Dry Powder Pulmonary Inhalation Delivery. Aaps Pharmscitech 12, 1420-1430.
599 Liggins, R.T., Hunter, W.L., Burt, H.M., 1997. Solid-State Characterization of Paclitaxel.
600 Journal of Pharmaceutical Sciences 86, 1459-1463.
601 Mansour, H., Wang, D.S., Chen, C.S., Zografi, G., 2001. Comparison of bilayer and monolayer
602 properties of phospholipid systems containing dipalmitoylphosphatidylglycerol and
603 dipalmitoylphosphatidylinositol. Langmuir 17, 6622-6632.
604 Mansour, H.M., Rhee, Y.-S., Wu, X., 2009. Nanomedicine in pulmonary delivery. International
605 Journal of Nanomedicine 4, 299-319.
606 Mansour, H.M., Rhee, Y.S., Park, C.W., DeLuca, P.P., 2011. Lipid Nanoparticulate Drug
607 Delivery and Nanomedicine, in: Moghis, A. (Ed.), Lipids in Nanotechnology. American Oil
608 Chemists Society (AOCS) Press, Urbana, Illinois, pp. 221-268.
609 Mansour, H.M., Sohn, M., Al-Ghananeem, A., DeLuca, P.P., 2010. Materials for Pharmaceutical
610 Dosage Forms: Molecular Pharmaceutics and Controlled Release Drug Delivery Aspects.
611 International Journal of Molecular Sciences 11, 3298-3322.
612 Mansour, H.M., Zografi, G., 2007a. The relationship between water vapor absorption and
613 desorption by phospholipids and bilayer phase transitions. Journal of Pharmaceutical Sciences
614 96, 377-396.
615 Mansour, H.M., Zografi, G., 2007b. Relationships between equilibrium spreading pressure and
616 phase equilibria of phospholipid bilayers and monolayers at the air-water interface. Langmuir 23,
617 3809-3819.
618 Marupudi, N.I., Han, J.E., Li, K.W., Renard, V.M., Tyler, B.M., Brem, H., 2007. Paclitaxel: a
619 review of adverse toxicities and novel delivery strategies. Expert Opinion on Drug Safety 6, 609-
620 621.
621 Meenach, S.A., Kim, Y.J., Kauffman, K.J., Kanthamneni, N., Bachelder, E.M., Ainslie, K.M.,
622 2012a. Synthesis, Optimization, and Characterization of Camptothecin-Loaded Acetalated
623 Dextran Porous Microparticles for Pulmonary Delivery. Molecular Pharmaceutics 9, 290-298.
624 Meenach, S.A., Vogt, F.G., Anderson, K.W., Hilt, J.Z., McGarry, R.C., Mansour, H.M., 2012b.
625 Design, physicochemical characterization, and optimization of organic solution advanced spray-
626 dried inhalable dipalmitoylphosphatidylcholine (DPPC) and
627 dipalmitoylphosphatidylethanolamine poly(ethylene glycol) (DPPE-PEG) microparticles and
628 nanoparticles for targeted respiratory nanomedicine delivery as dry powder inhalation aerosols.
629 International Journal of Nanomedicine 8, 275-293.
630 Pappalardo, M., Milardi, D., Grasso, D., La Rosa, C., 2005. Phase behaviour of polymer-grafted
631 DPPC membranes for drug delivery systems design. Journal of Thermal Analysis and
632 Calorimetry 80, 413-418.
633 Patton, J.S., Byron, P.R., 2007. Inhaling medicines: delivering drugs to the body through the
634 lungs. Nature Reviews Drug Discovery 6, 67-74.
635 Rhee, Y.S., Mansour, H.M., 2011. Nanopharmaceuticals I: nanocarrier systems in drug delivery.
636 International Journal of Nanotechnology 8, 84-114.
637 Sharma, S., White, D., Imondi, A., Placke, M.E., Vail, D.M., Kris, M.G., 2001. Development of
638 inhalation agents for oncologic use. Journal of Clinical Oncology 19, 1839-1847.

639 Suarez, S., Hickey, A.J., 2000. Drug properties affecting aerosol behavior. Respiratory Care 45,
640 652-666.
641 Sung, J.C., Pulliam, B.L., Edwards, D.A., 2007. Nanoparticles for drug delivery to the lungs.
642 Trends in Biotechnology 25, 563-570.
643 Tang, B.C., Fu, J., Watkins, D.N., Hanes, J., 2010. Enhanced efficacy of local etoposide delivery
644 by poly(ether-anhydride) particles against small cell lung cancer in vivo. Biomaterials 31, 339-
645 344.
646 Tomoda, K., Ohkoshi, T., Hirota, K., Sonavane, G.S., Nakajima, T., Terada, H., Komuro, M.,
647 Kitazato, K., Makino, K., 2009. Preparation and properties of inhalable nanocomposite particles
648 for treatment of lung cancer. Colloids and Surfaces B: Biointerfaces 71, 177-182.
649 Törmälä, P., 1974. Determination of glass transition temperature of poly(ethylene glycol) by spin
650 probe technique. European Polymer Journal 10, 519-521.
651 Vaughn, J.M., McConville, J.T., Burgess, D., Peters, J.I., Johnston, K.P., Talbert, R.L., Williams,
652 R.O., 2006. Sing dose and multiple dose studies of itraconazole nanoparticles. European Journal
653 of Pharmaceutics and Biopharmaceutics 63, 95-102.
654 Vehring, R., Foss, W.R., Lechuga-Ballesteros, D., 2007. Particle formation in spray drying.
655 Journal of Aerosol Science 38, 728-746.
656 Watts, A.B., McConville, J.T., Williams, R.O., 2008. Advancements in dry powder delivery to
657 the lung. Drug Development and Industrial Pharmacy 34, 948-959.
658 Wu, X.A., Li, X.J., Mansour, H.M., 2010. Surface Analytical Techniques in Solid-State Particle
659 Characterization for Predicting Performance in Dry Powder Inhalers. Kona Powder and Particle
660 Journal, 3-19.
661 Wu, X.A., Mansour, H.M., 2011. Nanopharmaceuticals II: application of nanoparticles and
662 nanocarrier systems in pharmaceutics and nanomedicine. International Journal of
663 Nanotechnology 8, 115-145.
664 Yang, T., Choi, M.-K., Cui, F.-D., Kim, J.S., Suk-Jae, C., Shim, C.-K., Kim, D.-D., 2007.
665 Preparation and evaluation of paclitaxel-loaded PEGylated immunoliposome. Journal of
666 Controlled Release 120, 169-177.
667 Yang, Y., Bajaj, N., Xu, P., Ohn, K., Tsifansky, M.D., Yeo, Y., 2009. Development of highly
668 porous large PLGA microparticles for pulmonary drug delivery. Biomaterials 30, 1947-1953.

669

670

671

## LIST OF TABLE LEGENDS

**Table I.** List of co-spray dried (co-SD) and single-component spray dried (SD) formulations and their corresponding outlet temperatures during spray drying, size, water content, and paclitaxel encapsulation efficiency (EE) and loading. (n = 3, Ave ± SD)

**Table II.** Next Generation Impactor™ results for co-spray dried (co-SD) and one-component spray dried (SD) aerosol systems including mass median aerodynamic diameter (MMAD), geometric standard deviation (GSD), fine particle fraction (FPF) below 4.4 μm, respirable fraction (RF) below 4.4 μm, and emitted dose (ED). (n = 3, Ave ± SD)

## LIST OF FIGURE LEGENDS

**Figure 1.** SEM micrographs of co-spray dried (co-SD) PEGylated phospholipid particles with varying PEG chain length containing 5% paclitaxel (PTX): (a) co-SD 5PTX:95DPPC; (b) co-SD 5PTX:95DPPC/DPPE-PEG2k; (c) co-SD 5PTX:95DPPC/DPPE-PEG3k; and (d) co-SD 5PTX:95DPPC:DPPE-PEG5k. Magnification for all samples was 10,000x.

**Figure 2.** SEM micrographs of co-spray dried (co-SD) PEGylated phospholipid particles with varying PEG chain length containing 25% paclitaxel (PTX): (a) co-SD 25PTX:75DPPC; (b) co-SD 25PTX:75DPPC/DPPE-PEG2k; (c) co-SD 25PTX:75DPPC/DPPE-PEG3k; and (d) co-SD 25PTX:75DPPC/DPPE-PEG5k. Magnification for all samples was 10,000x.

**Figure 3.** SEM micrographs of co-spray dried (co-SD) PEGylated phospholipid particles with varying PEG chain length containing 50% paclitaxel (PTX): (a) co-SD 50PTX:50DPPC; (b) co-SD 50PTX:50DPPC/DPPE-PEG2k; (c) co-SD 50PTX:50DPPC/DPPE-PEG3k; and (d) co-SD 50PTX:50DPPC/DPPE-PEG5k. Magnification for all samples was 10,000x.

**Figure 4.** SEM micrographs of co-spray dried (co-SD) PEGylated phospholipid particles with varying PEG chain length containing 75% paclitaxel (PTX): (a) co-SD 75PTX:25DPPC; (b) co-SD 75PTX:25DPPC/DPPE-PEG2k; (c) co-SD 75PTX:25DPPC/DPPE-PEG3k; and (d) co-SD 75PTX:25DPPC/DPPE-PEG5k. Magnification for all samples was 10,000x.

**Figure 5.** SEM micrographs of spray-dried (SD) 100% paclitaxel particles (100PTX) following spray drying at three pump rates (Low P, Med P, and High P) for: (a) Raw paclitaxel (PTX); (b) SD 100PTX (Low P); (c) SD 100PTX (Med P); and (d) SD 100PTX (High P). Magnification for all samples was 10,000x.

**Figure 6.** DSC thermograms of spray-dried (SD) and co-spray-dried (co-SD) particles with varying PTX content and PEG chain lengths for: (a) co-SD 5PTX:95 DPPC *vs.* co-SD 5PTX:95 DPPC/DPPE-PEG; (b) co-SD 25 PTX:75 DPPC *vs.* co-SD 25 PTX:75 DPPC/DPPE-PEG; (c) co-SD 50PTX:50 DPPC *vs.* co-SD 50 PTX:50 DPPC/DPPE-PEG; (d) co-SD 75PTX:25 DPPC

713 *vs.* co-SD 75PTX:25DPPC/DPPE-PEG; (e) SD 100PTX from three pump rates *vs.* raw PTX; and
714 (f) insert of co-SD 75PTX:25 DPPC *vs.* co-SD 75PTX:25DPPC/DPPE-PEG for $T_g$ transition
715 visualization.
716
717 **Figure 7.** X-ray powder diffractograms of spray-dried (SD) and co-spray-dried (co-SD)
718 particles with varying PTX content and PEG chain lengths for: (a) co-SD 5PTX:95 DPPC *vs.*
719 co-SD 5PTX:95 DPPC/DPPE-PEG; (b) co-SD 25 PTX:75 DPPC *vs.* co-SD 25 PTX:75
720 DPPC/DPPE-PEG; (c) co-SD 50PTX:50 DPPC *vs.* co-SD 50 PTX:50 DPPC/DPPE-PEG; (d)
721 co-SD 75PTX:25 DPPC *vs.* co-SD 75PTX:25DPPC/DPPE-PEG; and (e) SD 100PTX at three
722 pump rates *vs.* raw PTX.
723
724 **Figure 8.** Representative ATR-FTIR spectra of co-spray-dried (co-SD) PTX:DPPC/DPPE-
725 PEG3k particles in comparison to raw DPPC and raw paclitaxel.
726
727 **Figure 9**. Representative HSM micrographs of co-spray dried (co-SD) for: (a) co-SD
728 5PTX:95DPPC/DPPE-PEG3k; and (b) co-SD 50PTX:50DPPC/DPPE-PEG3k particles (scale bar
729 = 3 mm).
730
731 **Figure 10**. Representative HSM micrographs of spray-dried (SD): (a) SD 100PTX (High P)
732 particles; and (b) raw paclitaxel. (Scale bar = 3 mm).
733
734 **Figure 11**. Aerosol dispersion performance as % deposited on each stage of the Next Generation
735 Impactor™ (NGI™) for spray-dried (SD) and co-spray-dried (co-SD) particles with varying
736 PTX content and PEG chain lengths for: a) co-SD 5PTX:95 DPPC *vs.* co-SD 5PTX:95
737 DPPC/DPPE-PEG; b) co-SD 25 PTX:75 DPPC *vs.* co-SD 25 PTX:75 DPPC/DPPE-PEG; c) co-
738 SD 50PTX:50 DPPC *vs.* co-SD 50 PTX:50 DPPC/DPPE-PEG; d) co-SD 75PTX:25 DPPC *vs.*
739 co-SD 75PTX:25DPPC/DPPE-PEG; and e) SD 100PTX particles spray-dried at three pump
740 rates (Low P, Med P, and High P). For Q= 60 L/minute, the effective cutoff diameters for each
741 NGI™ impaction stage are as follows: Stage 1 (8.06 μm); Stage 2 (4.46 μm); Stage 3 (2.82 μm);

742 Stage 4 (1.66 μm); Stage 5 (0.94 μm); Stage 6 (0.55 μm); and Stage 7 (0.34 μm). (n = 3, Ave ±
743 SD)

744 **Table I.** List of co-spray dried (co-SD) and single-component spray dried (SD) formulations
745 and their corresponding outlet temperatures during spray drying, size, water content, and
746 paclitaxel encapsulation efficiency (EE) and loading. (n = 3, Ave ± SD)

| System | Outlet T (°C) | Size (μm) | Water (%) | PTX EE (%) | PTX Loading (μg PTX/mg particle) |
|---|---|---|---|---|---|
| 5PTX:95DPPC | 50 | 0.946 ± 0.427 | 3.60 ± 0.37 | 99.0 ± 0.3 | 60.2 ± 1.5 |
| 5PTX:95DPPC/DPPE-PEG2k | 52 | 1.095 ± 0.458 | 4.30 ± 0.20 | 95.0 ± 0.2 | 48.4 ± 0.8 |
| 5PTX:95DPPC/DPPE-PEG3k | 54 | 0.963 ± 0.431 | 2.44 ± 0.78 | 99.6 ± 0.2 | 48.2 ± 0.1 |
| 5PTX:95DPPC/DPPE-PEG5k | 55 | 1.567 ± 0.673 | 2.25 ± 0.44 | 94.7 ± 0.2 | 41.3 ± 0.9 |
| 25PTX:75DPPC | 56 | 1.539 ± 0.661 | 3.73 ± 0.96 | 88.5 ± 0.1 | 191.4 ± 0.3 |
| 25PTX:75DPPC/DPPE-PEG2k | 55 | 3.416 ± 0.808 | 4.58 ± 1.31 | 82.3 ± 0.3 | 209.2 ± 0.9 |
| 25PTX:75DPPC/DPPE-PEG3k | 55 | Not measurable | 2.21 ± 0.18 | 99.5 ± 0.4 | 242.6 ± 1.1 |
| 25PTX:75DPPC/DPPE-PEG5k | 54 | Not measurable | 1.47 ± 0.18 | 95.0 ± 0.4 | 212.9 ± 0.9 |
| 50PTX:50DPPC | 50 | 0.801 ± 0.230 | 3.85 ± 0.68 | 85.0 ± 0.4 | 511.0 ± 2.0 |
| 50PTX:50DPPC/DPPE-PEG2k | 51 | 1.001 ± 0.316 | 6.78 ± 1.18 | 62.7 ± 0.4 | 316.8 ± 1.8 |
| 50PTX:50DPPC/DPPE-PEG3k | 50 | 1.215 ± 0.394 | 3.27 ± 0.27 | 73.0 ± 0.4 | 359.1 ± 1.8 |
| 50PTX:50DPPC/DPPE-PEG5k | 52 | Not measurable | 5.78 ± 0.40 | 71.2 ± 0.4 | 330.8 ± 1.8 |
| 75PTX:25DPPC | 38 | 0.778 ± 0.306 | 3.78 ± 0.89 | 87.5 ± 0.4 | 679.9 ± 2.9 |
| 75PTX:25DPPC/DPPE-PEG2k | 38 | 0.781 ± 0.307 | 5.86 ± 0.38 | 84.6 ± 0.4 | 638.2 ± 3.1 |
| 75PTX:25DPPC/DPPE-PEG3k | 33 | 0.876 ± 0.337 | 1.60 ± 0.62 | 76.8 ± 0.4 | 571.2 ± 3.2 |
| 75PTX:25DPPC/DPPE-PEG5k | 35 | 0.765 ± 0.377 | 4.60 ± 0.21 | 82.4 ± 0.2 | 644.7 ± 1.5 |
| 100PTX (Low P) | 73 | 0.631 ± 0.265 | 2.28 ± 0.11 | n/a | n/a |
| 100PTX (Med P) | 81 | 0.624 ± 0.247 | 1.41 ± 0.38 | n/a | n/a |
| 100PTX (High P) | 41 | 0.672 ± 0.274 | 0.44 ± 0.39 | n/a | n/a |

747

748 **Table II.** Next Generation Impactor™ results for co-spray dried (co-SD) and one-component
749 spray dried (SD) aerosol systems including mass median aerodynamic diameter (MMAD),
750 geometric standard deviation (GSD), fine particle fraction (FPF) below 4.4 μm, respirable
751 fraction (RF) below 4.4 μm, and emitted dose (ED). (n = 3, Ave ± SD)

| System | MMAD (μm) | GSD (μm) | Fine Particle Fraction (%) | Respirable Fraction (%) | Emitted Dose (%) |
|---|---|---|---|---|---|
| 5PTX:95DPPC | 3.4 | 2.4 | 77.9 ± 7.0 | 50.3 ± 0.5 | 80.0 ± 4.0 |
| 5PTX:95DPPC/DPPE-PEG2k | 4.7 | 2.4 | 60.1 ± 8.0 | 49.2 ± 2.6 | 89.8 ± 1.7 |
| 5PTX:95DPPC/DPPE-PEG3k | 4.9 | 2.9 | 64.1 ± 6.8 | 47.5 ± 6.7 | 90.8 ± 0.1 |
| 5PTX:95DPPC/DPPE-PEG5k | 7.5 | 3.8 | 43.3 ± 2.2 | 44.0 ± 0.5 | 94.5 ± 1.0 |
| 25PTX:75DPPC | 3.3 | 2.3 | 75.4 ± 4.0 | 52.4 ± 2.1 | 88.6 ± 6.1 |
| 25PTX:75DPPC/DPPE-PEG2k | 4.0 | 2.6 | 64.5 ± 2.0 | 51.7 ± 4.5 | 95.2 ± 2.5 |
| 25PTX:75DPPC/DPPE-PEG3k | 4.5 | 2.4 | 58.1 ± 8.0 | 49.1 ± 6.4 | 91.1 ± 3.4 |
| 25PTX:75DPPC/DPPE-PEG5k | 6.8 | 3.1 | 55.4 ± 1.0 | 48.8 ± 7.1 | 92.2 ± 6.1 |
| 50PTX:50DPPC | 3.1 | 2.5 | 65.8 ± 2.4 | 53.4 ± 1.3 | 90.1 ± 4.1 |
| 50PTX:50DPPC/DPPE-PEG2k | 3.8 | 2.4 | 67.5 ± 2.7 | 54.4 ± 6.2 | 91.1 ± 4.1 |
| 50PTX:50DPPC/DPPE-PEG3k | 4.2 | 2.8 | 62.7 ± 3.6 | 51.9 ± 2.5 | 94.5 ± 5.2 |
| 50PTX:50DPPC/DPPE-PEG5k | 5.3 | 3.1 | 62.8 ± 7.2 | 49.9 ± 4.2 | 97.9 ± 3.2 |
| 75PTX:25DPPC | 2.7 | 2.0 | 73.2 ± 6.3 | 52.5 ± 6.1 | 89.8 ± 3.3 |
| 75PTX:25DPPC/DPPE-PEG2k | 3.9 | 2.3 | 72.3 ± 4.7 | 53.1 ± 1.1 | 91.5 ± 3.9 |
| 75PTX:25DPPC/DPPE-PEG3k | 4.0 | 2.8 | 69.9 ± 2.9 | 54.5 ± 2.2 | 96.7 ± 7.1 |
| 75PTX:25DPPC/DPPE-PEG5k | 4.8 | 3.4 | 63.2 ± 4.4 | 54.1 ± 2.0 | 94.3 ± 5.2 |
| 100PTX (Low) | 3.2 | 2.3 | 70.6 ± 2.1 | 59.9 ± 0.8 | 90.2 ± 4.7 |
| 100PTX (Med) | 3.3 | 2.5 | 64.6 ± 1.3 | 66.6 ± 3.1 | 85.1 ± 9.0 |
| 100PTX (High) | 3.4 | 2.6 | 68.3 ± 1.1 | 65.7 ± 0.2 | 89.3 ± 3.2 |

752

753

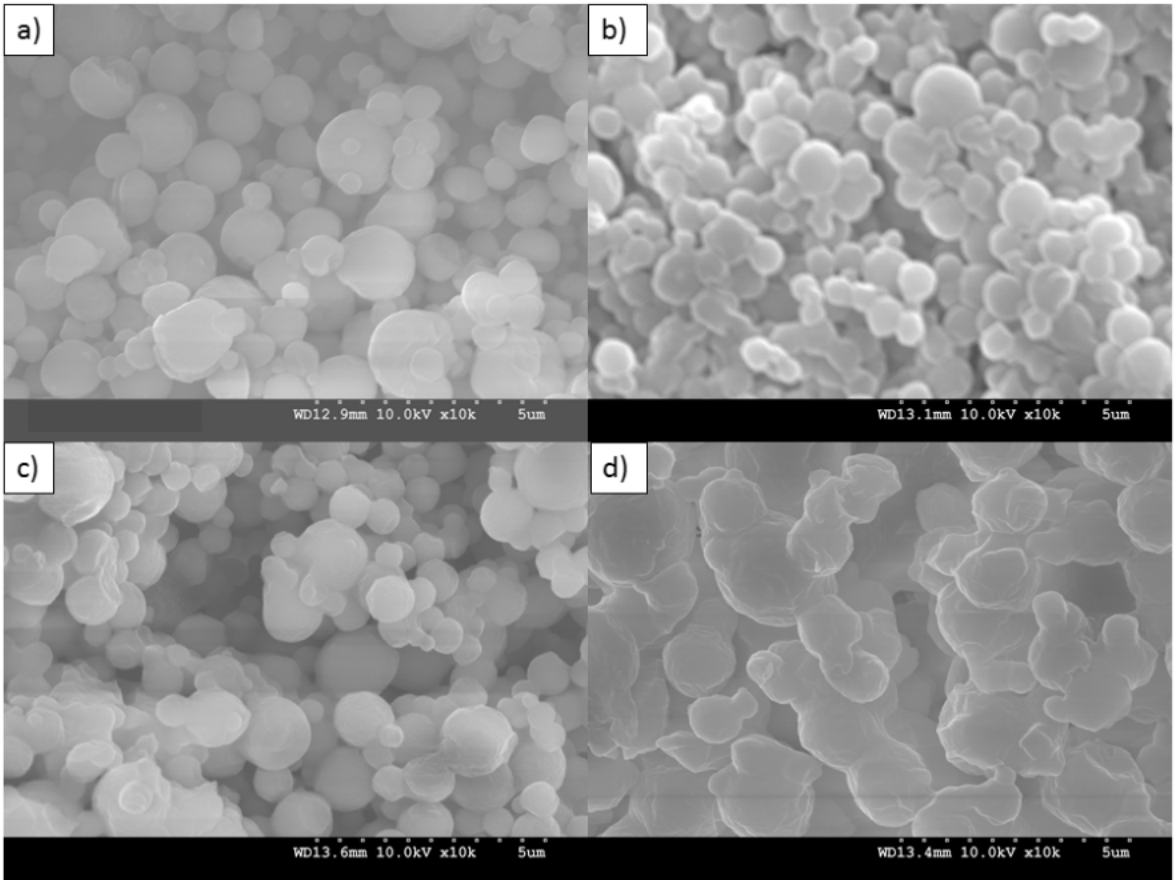


**Figure 1.** SEM micrographs of co-spray dried (co-SD) PEGylated phospholipid particles with varying PEG chain length containing 5% paclitaxel (PTX): (a) co-SD 5PTX:95DPPC; (b) co-SD 5PTX:95DPPC/DPPE-PEG2k; (c) co-SD 5PTX:95DPPC/DPPE-PEG3k; and (d) co-SD 5PTX:95DPPC:DPPE-PEG5k. Magnification for all samples was 10,000x.

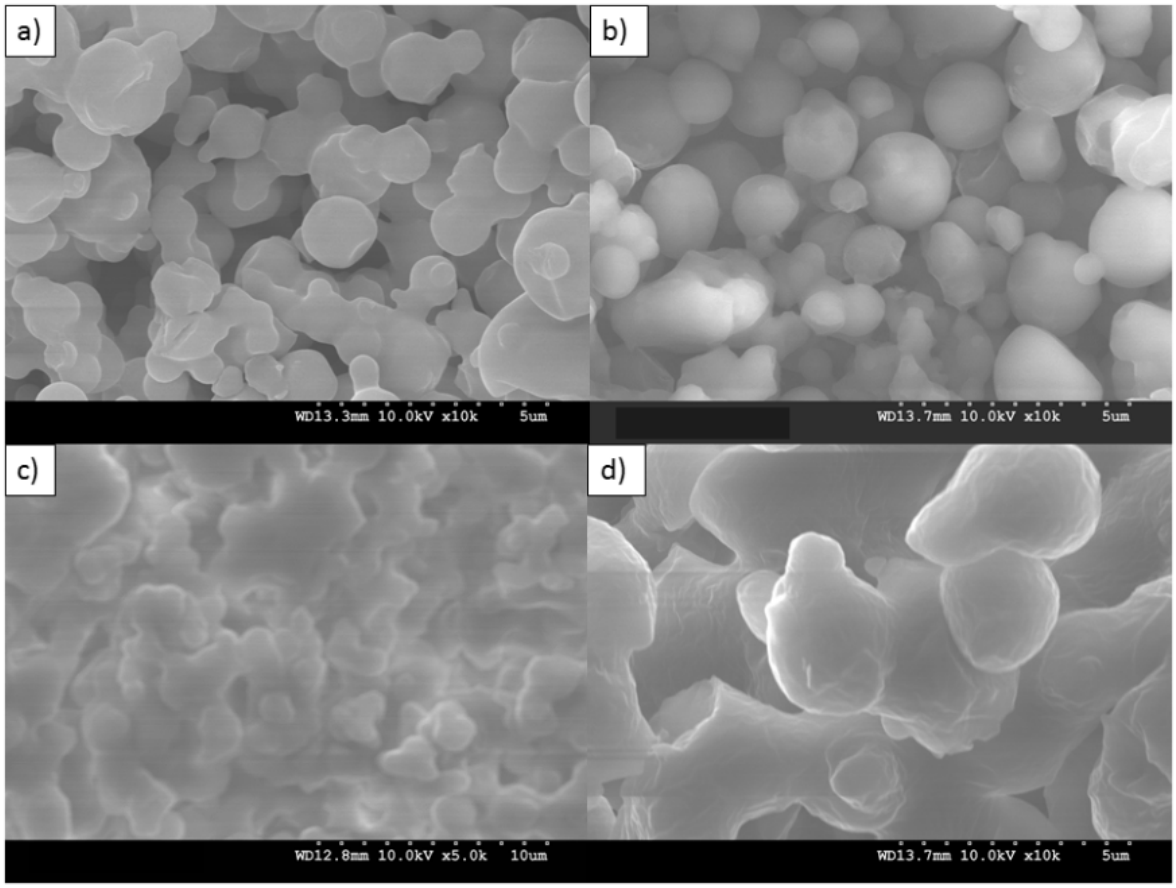


**Figure 2.** SEM micrographs of co-spray dried (co-SD) PEGylated phospholipid particles with varying PEG chain length containing 25% paclitaxel (PTX): (a) co-SD 25PTX:75DPPC; (b) co-SD 25PTX:75DPPC/DPPE-PEG2k; (c) co-SD 25PTX:75DPPC/DPPE-PEG3k; and (d) co-SD 25PTX:75DPPC/DPPE-PEG5k. Magnification for all samples was 10,000x.

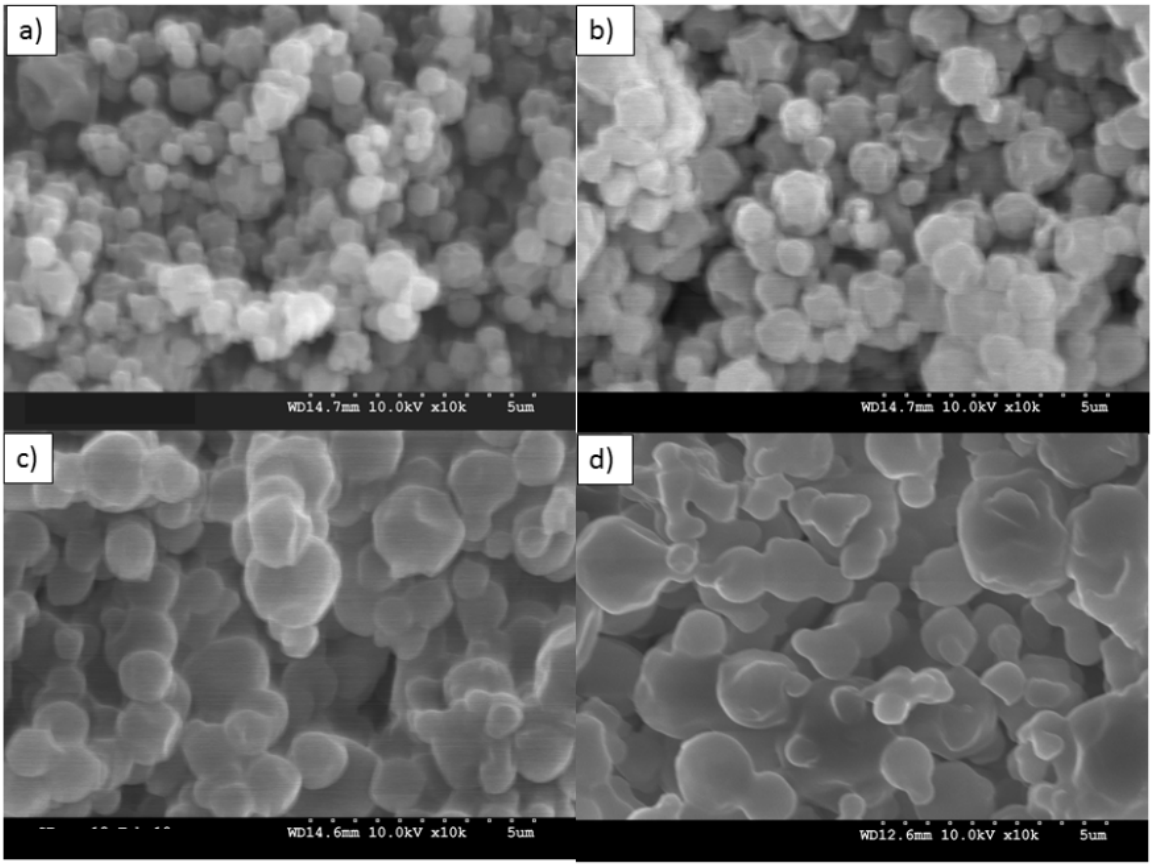


766

767 **Figure 3.** SEM micrographs of co-spray dried (co-SD) PEGylated phospholipid particles with
768 varying PEG chain length containing 50% paclitaxel (PTX): (a) co-SD 50PTX:50DPPC; (b) co-
769 SD 50PTX:50DPPC/DPPE-PEG2k; (c) co-SD 50PTX:50DPPC/DPPE-PEG3k; and (d) co-SD
770 50PTX:50DPPC/DPPE-PEG5k. Magnification for all samples was 10,000x.

771

772

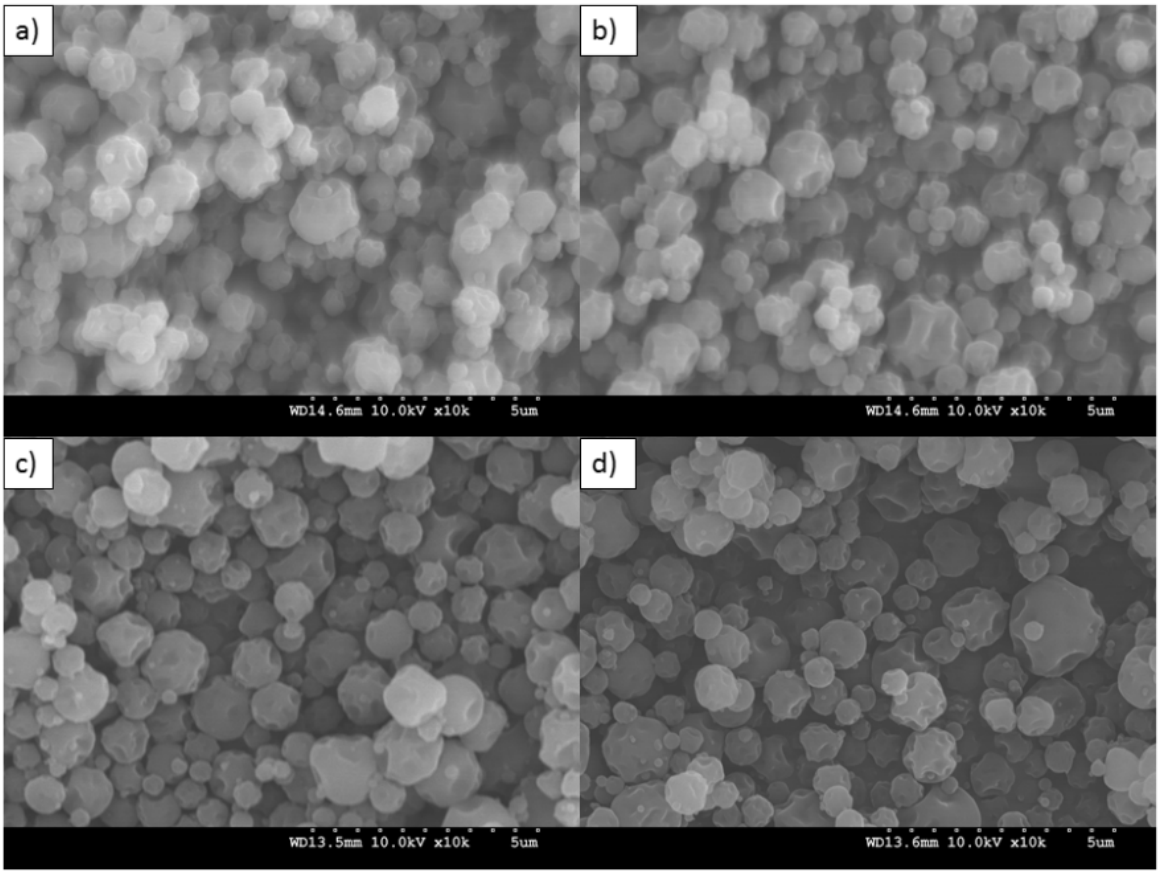


**Figure 4.** SEM micrographs of co-spray dried (co-SD) PEGylated phospholipid particles with varying PEG chain length containing 75% paclitaxel (PTX): (a) co-SD 75PTX:25DPPC; (b) co-SD 75PTX:25DPPC/DPPE-PEG2k; (c) co-SD 75PTX:25DPPC/DPPE-PEG3k; and (d) co-SD 75PTX:25DPPC/DPPE-PEG5k. Magnification for all samples was 10,000x.

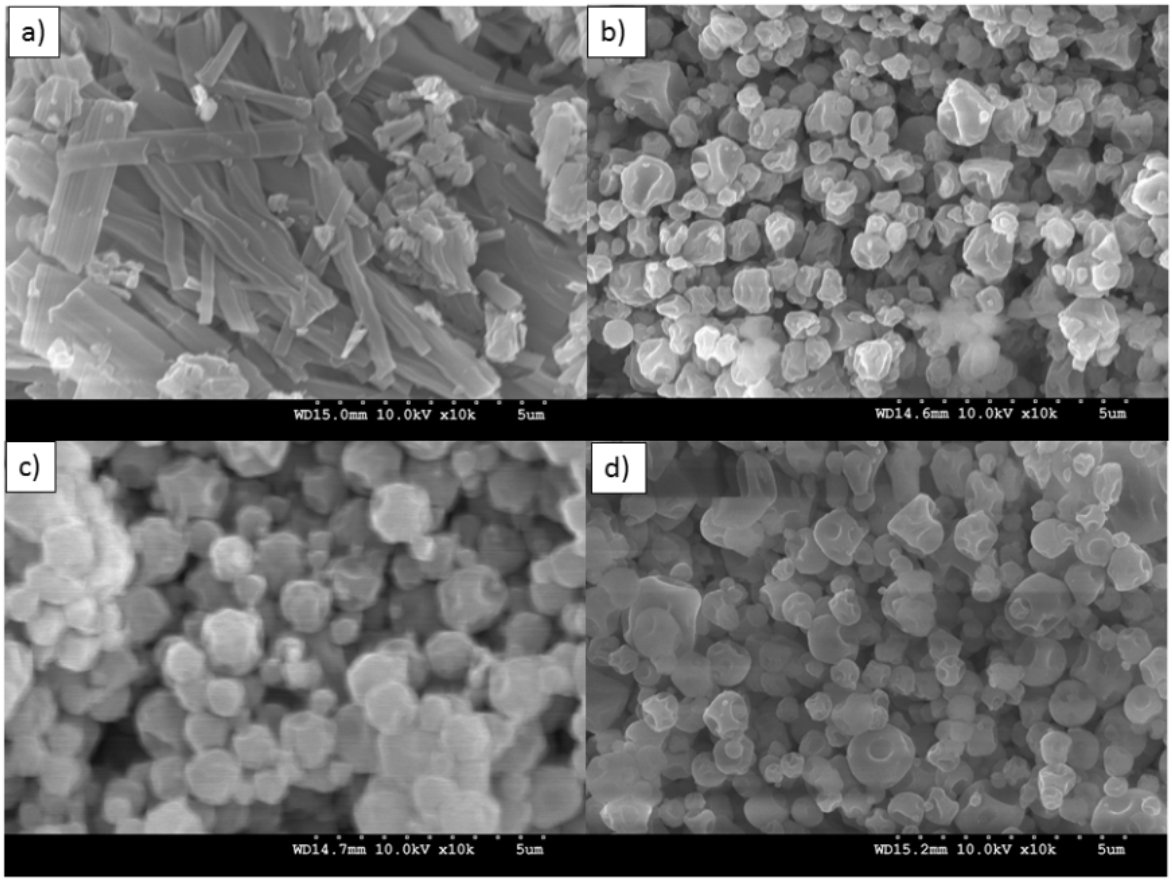


**Figure 5.** SEM micrographs of spray-dried (SD) paclitaxel particles (100PTX) following spray drying at three pump rates (Low P, Med P, and High P): (a) Raw paclitaxel (PTX); (b) SD 100PTX (Low P); (c) SD 100PTX (Med P); and (d) SD 100PTX (High P). Magnification for all samples was 10,000x.

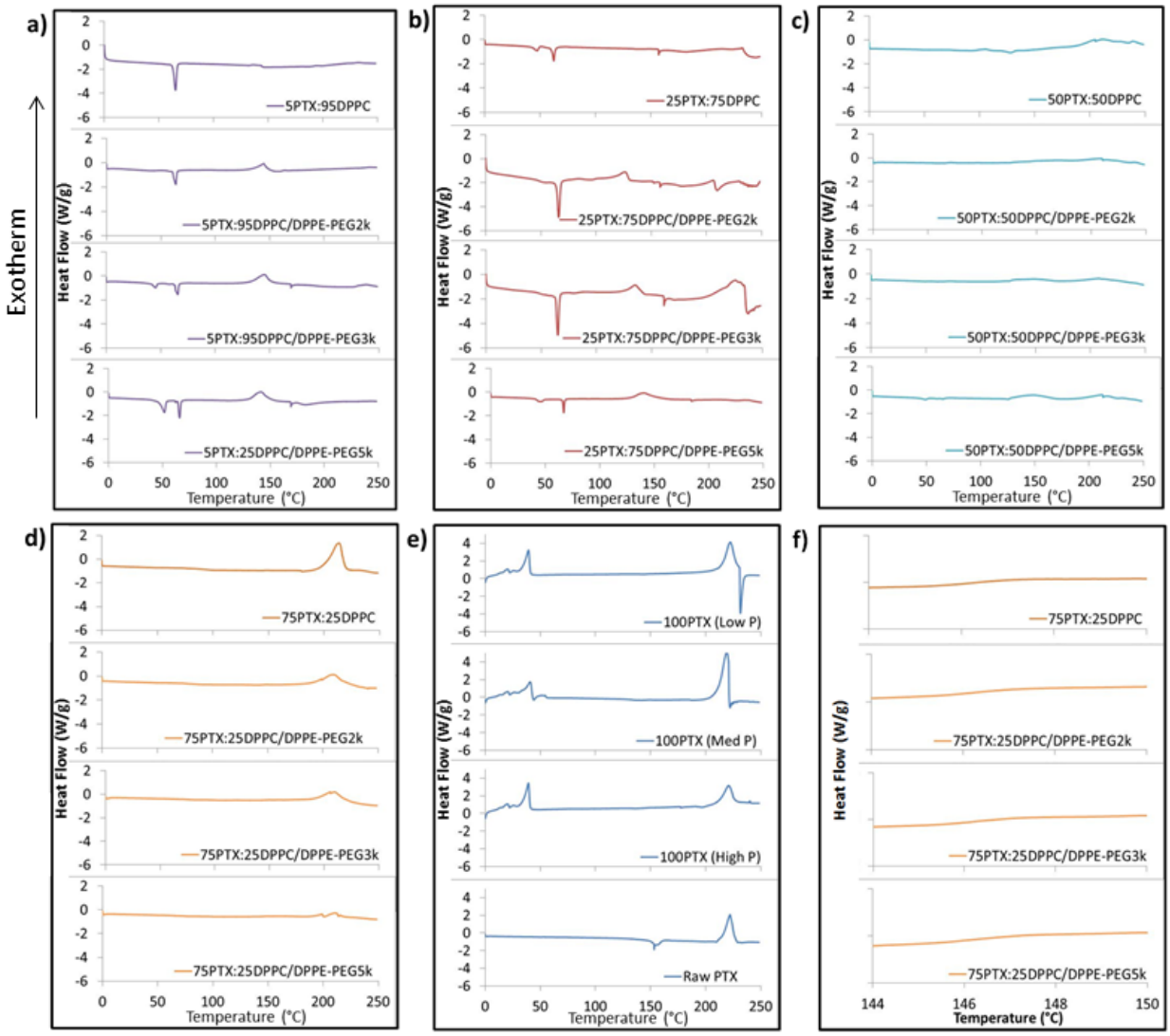


**Figure 6.** DSC thermograms of spray-dried (SD) and co-spray-dried (co-SD) particles with varying PTX content and PEG chain lengths for: (a) co-SD 5PTX:95 DPPC *vs.* co-SD 5PTX:95 DPPC/DPPE-PEG; (b) co-SD 25 PTX:75 DPPC *vs.* co-SD 25 PTX:75 DPPC/DPPE-PEG; (c) co-SD 50PTX:50 DPPC *vs.* co-SD 50 PTX:50 DPPC/DPPE-PEG; (d) co-SD 75PTX:25 DPPC *vs.* co-SD 75PTX:25DPPC/DPPE-PEG; (e) SD 100PTX from three pump rates *vs.* raw PTX; and (f) insert of co-SD 75PTX:25 DPPC *vs.* co-SD 75PTX:25DPPC/DPPE-PEG for $T_g$ transition visualization.

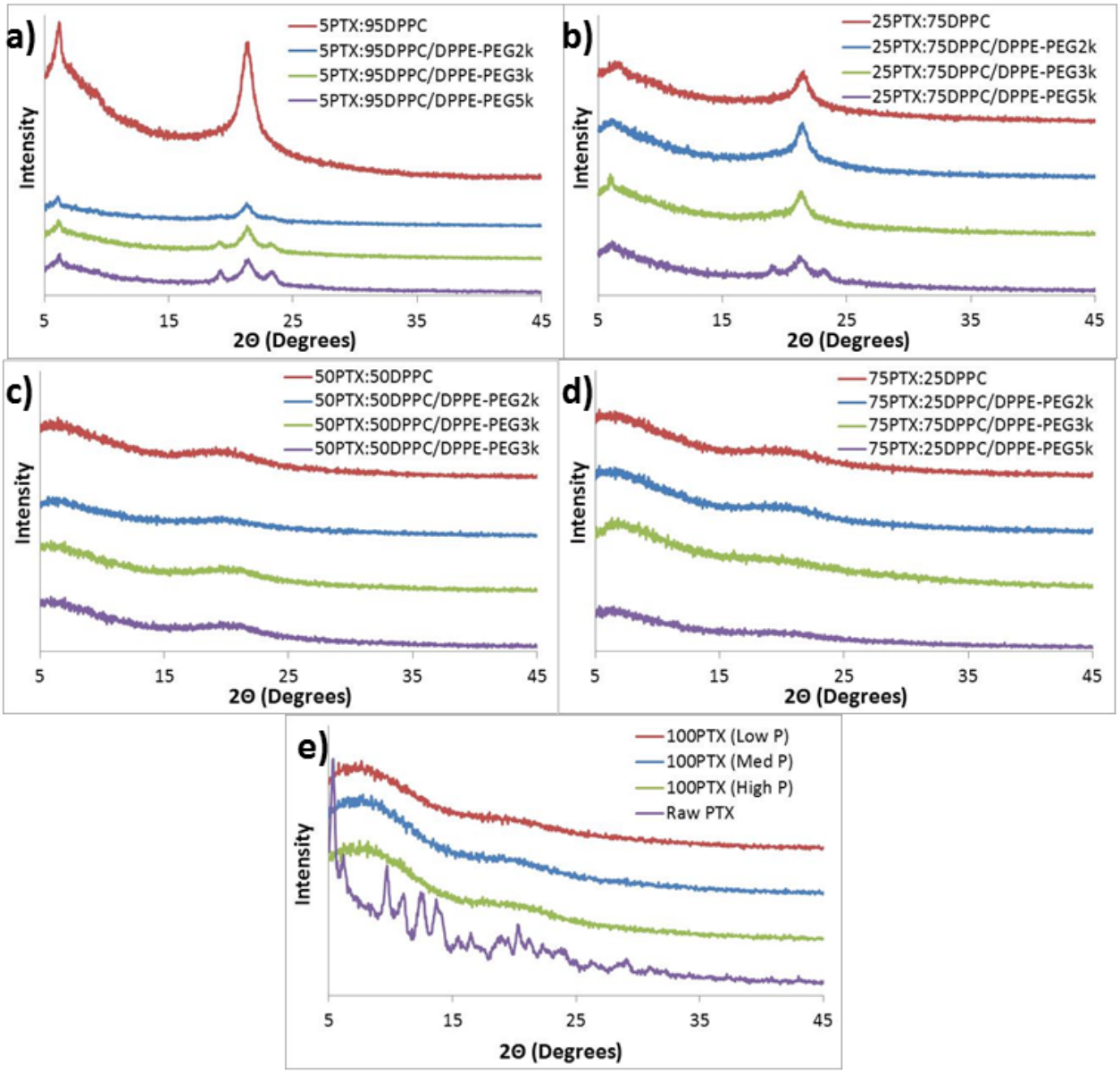


**Figure 7.** X-ray powder diffractograms of spray-dried (SD) and co-spray-dried (co-SD) particles with varying PTX content and PEG chain lengths for: (a) co-SD 5PTX:95 DPPC *vs.* co-SD 5PTX:95 DPPC/DPPE-PEG; (b) co-SD 25 PTX:75 DPPC *vs.* co-SD 25 PTX:75 DPPC/DPPE-PEG; (c) co-SD 50PTX:50 DPPC *vs.* co-SD 50 PTX:50 DPPC/DPPE-PEG; (d) co-SD 75PTX:25 DPPC *vs.* co-SD 75PTX:25DPPC/DPPE-PEG; and (e) SD 100PTX from three pump rates *vs.* raw PTX.

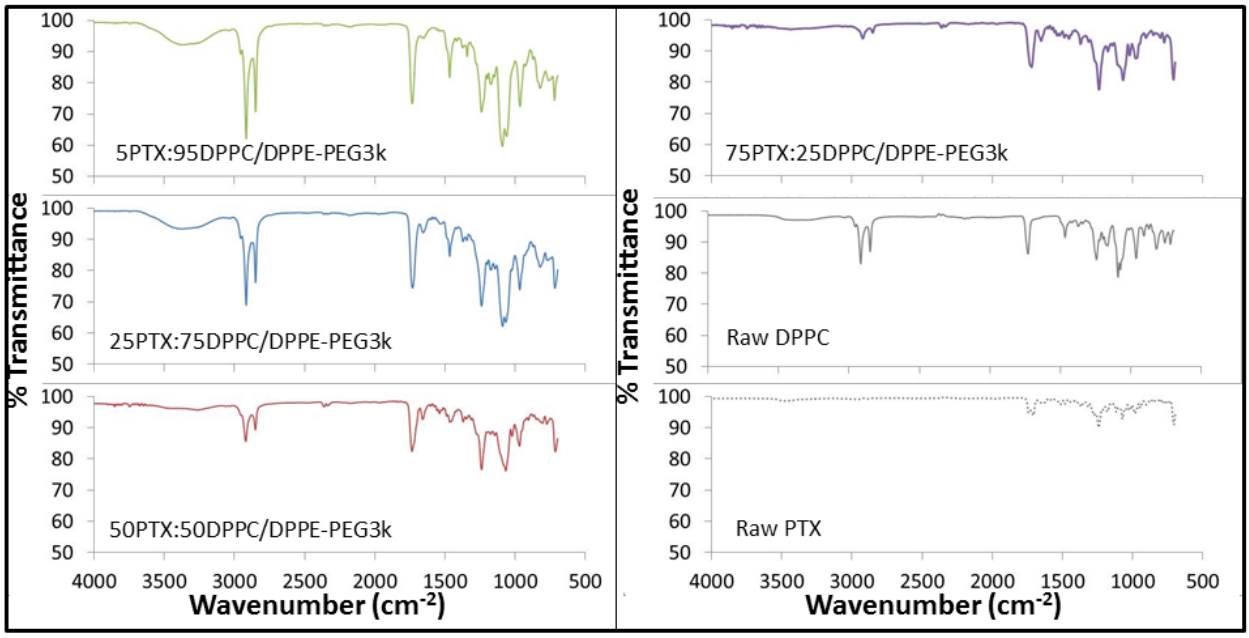


**Figure 8.** Representative ATR-FTIR spectra of co-spray-dried (co-SD) PTX:DPPC/DPPE-PEG3k particles in comparison to raw DPPC and raw paclitaxel.

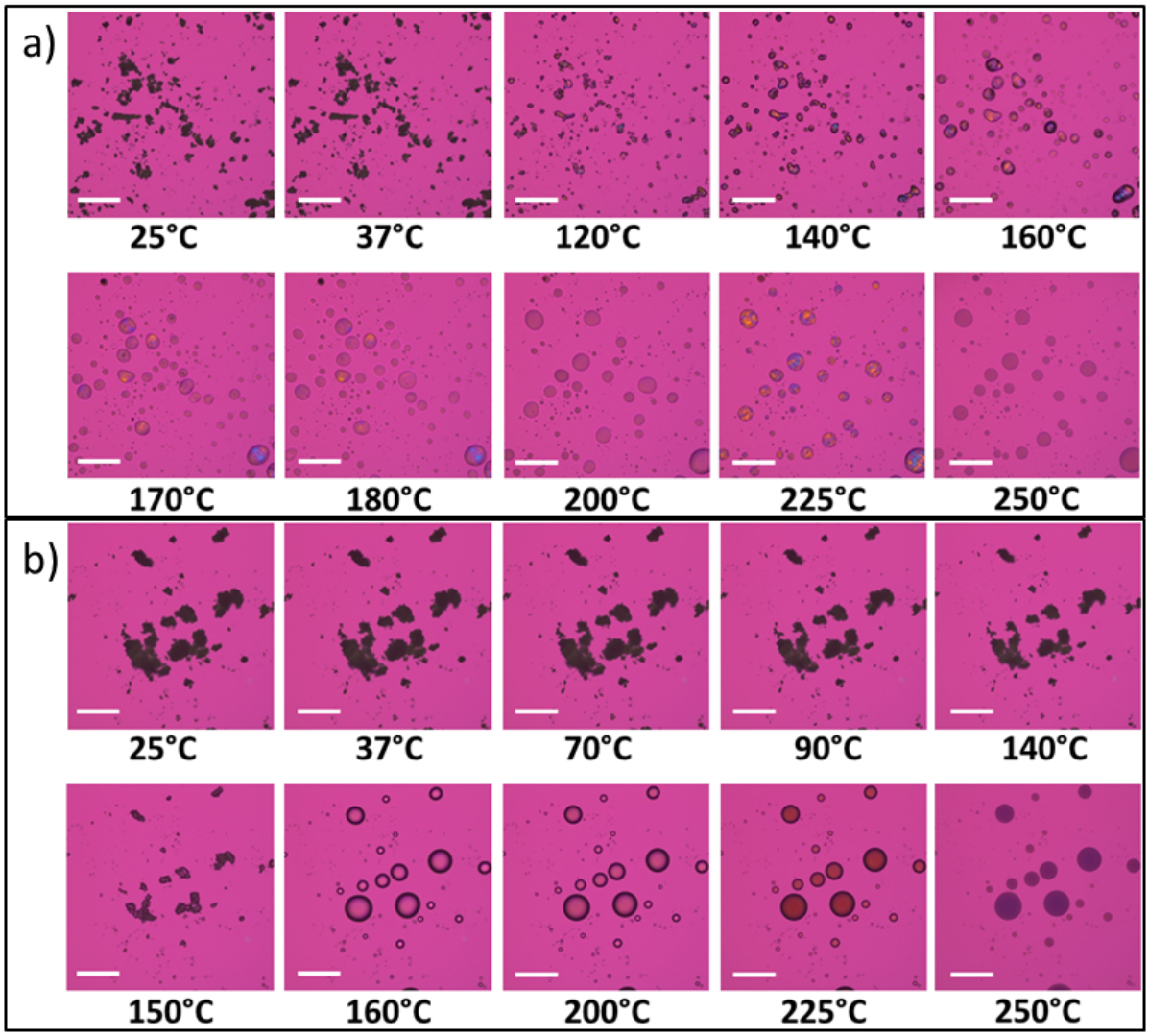


**Figure 9**. Representative HSM micrographs of co-spray dried (co-SD) for: (a) co-SD 5PTX:95DPPC/DPPE-PEG3k; and (b) co-SD 50PTX:50DPPC/DPPE-PEG3k particles (scale bar = 3 mm).

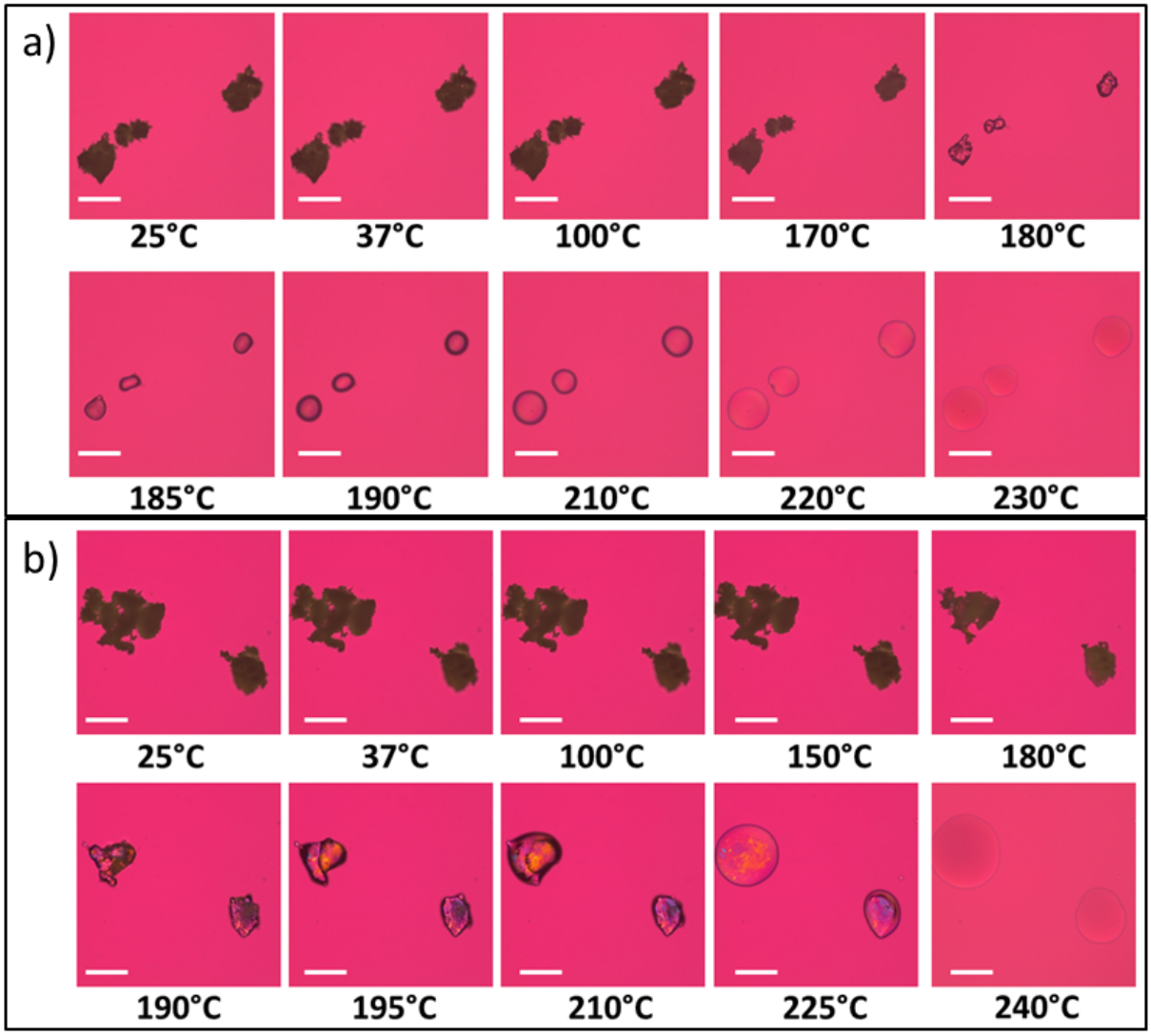


**Figure 10**. Representative HSM micrographs of spray-dried (SD): (a) SD 100PTX (High P) particles; and (b) raw paclitaxel. (Scale bar = 3 mm).

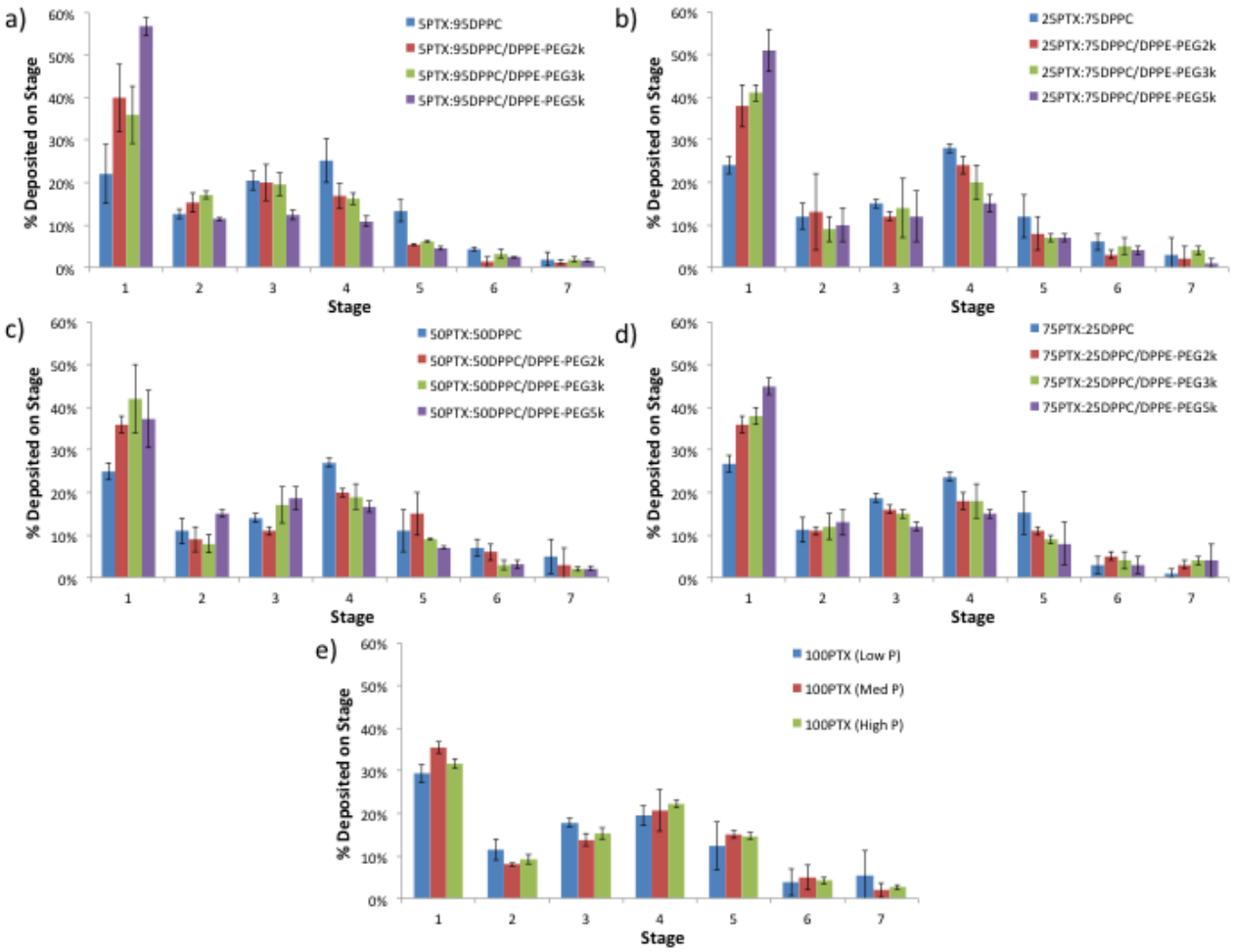


**Figure 11**. Aerosol dispersion performance as % deposited on each stage of the Next Generation Impactor™ (NGI™) for spray-dried (SD) and co-spray-dried (co-SD) particles with varying PTX content and PEG chain lengths for: a) co-SD 5PTX:95 DPPC *vs.* co-SD 5PTX:95 DPPC/DPPE-PEG; b) co-SD 25 PTX:75 DPPC *vs.* co-SD 25 PTX:75 DPPC/DPPE-PEG; c) co-SD 50PTX:50 DPPC *vs.* co-SD 50 PTX:50 DPPC/DPPE-PEG; d) co-SD 75PTX:25 DPPC *vs.* co-SD 75PTX:25DPPC/DPPE-PEG; and e) SD 100PTX particles spray-dried at three pump rates (Low P, Med P, and High P). For Q= 60 L/minute, the effective cutoff diameters for each NGI™ impaction stage are as follows: Stage 1 (8.06 µm); Stage 2 (4.46 µm); Stage 3 (2.82 µm); Stage 4 (1.66 µm); Stage 5 (0.94 µm); Stage 6 (0.55 µm); and Stage 7 (0.34 µm). (n = 3, Ave ± SD)